Contents lists available at ScienceDirect

Ore Geology Reviews

journal homepage: www.elsevier.com

Genesis of the Huangshannan high-Ni tenor magmatic sulfide deposit in the Eastern Tianshan, northwest China: Constraints from PGE geochemistry and Os–S isotopes

Ya-Jing Mao[a, b, *], Ke-Zhang Qin[a, *], Stephen J. Barnes[b], Dong-Mei Tang[a], Sheng-Chao Xue[a, c], Margaux Le Vaillant[b]

[a] Key Laboratory of Mineral Resources, Institute of Geology and Geophysics, Chinese Academy of Sciences, Beijing 100029, China
[b] CSIRO Mineral Resources, Perth 6151, Australia
[c] State Key Laboratory of Geological Processes and Mineral Resources, China University of Geosciences, Beijing 100083, China

ARTICLE INFO

Article history:
Received 5 December 2016
Received in revised form 15 March 2017
Accepted 16 May 2017
Available online xxx

Keywords:
Magmatic Ni-Cu sulfide deposit
High-Ni tenor
Pt and Pt anomaly
Huangshannan
Eastern Tianshan

ABSTRACT

The Huangshannan magmatic Ni-Cu sulfide deposit is one of a group of Permian magmatic Ni-Cu deposits located in the southern Central Asian Orogenic belt in the Eastern Tianshan, northwest China. It is characterized by elevated Ni tenor (concentrations in recalculated 100% sulfide) in sulfide within ultramafic rocks (9–19 wt%), with values much higher than other deposits in the region. Sulfides of the Huangshannan deposit are composed of pentlandite, chalcopyrite, and pyrrhotite and the host rock is relatively fresh, indicating that the high-Ni tenor is a primary magmatic feature rather than formed by alteration processes. It is shown that sulfides with high-Ni tenor can be generated by sulfide-olivine equilibrium at an oxygen fugacity of QFM +0.5, for magmas containing 450 ppm Ni and 20% olivine. Ores with >10 wt% sulfur have relatively low PGE and Ni tenors compared to other ores, R factor (mass ratio of silicate to sulfide liquid) modeling of Ni indicates that they formed at moderate R values (150–600). Based on this constraint on R values, ores with <10 wt% sulfides in the Huangshannan deposit can be segregated from a similar parental magma with 0.05 ppb Os, 0.023 ppb Ir, and 0.5 ppb Pd at R values between 600 and 3000. This, coupled with the supra-cotectic proportions of sulfide liquid to cumulus silicates in the Huangshannan ores imply mechanical transport and deposition of sulfide liquid in a magma pathway or conduit, in which sulfides must have interacted with large volumes of silicate magma. Platinum and Pd depletion relative to other platinum group elements (PGEs) are observed in fresh and sulfide-rich samples (S > 4.5 wt%). As sulfide-rich samples are also depleted in Cu, and as interstitial sulfides in those samples are physically interconnected at a scale of several cms, the low Pt and Pd anomalies are attributed to monosulfide solid solution (MSS) fractionation and Cu-rich sulfide liquid percolation during MSS fractionation. This finding indicates that Pt anomalies in sulfide-rich rocks from magmatic Ni-Cu deposits in the Eastern Tianshan are the result of sulfide fractionation rather than a hydrothermal effect. $^{187}Os/^{188}Os_{(278Ma)}$ values of the lherzolite samples vary from 0.27 to 0.37 and $\gamma Os_{(278Ma)}$ values vary from 110 to 189, indicating significant magma interaction with crustal sulfides, rich in radiogenic Os. Well constrained γOs values and $\delta^{34}S$ values (−0.4 to 0.8‰) indicate that crustal contamination occurred at depth before the arrival of the magma in the Huangshannan chamber. Regionally, deposits with high-Ni tenor have not been reported other than the Huangshannan deposit; however, many intrusions with high-Ni contents in olivine are present in NW China, such as the Erhongwa, Poyi and Poshi intrusions. Those intrusions are capable of forming high-Ni tenor sulfides due to olivine-sulfide-silicate equilibrium and relative high-Ni content in parent magma, making them attractive exploration targets.

1. Introduction

Magmatic Ni-Cu sulfide deposits can be divided into two major classes in terms of sulfide composition and Ni/Cu ratios (Barnes and Lightfoot, 2005). The Ni-poor class has Ni/Cu between 0.8 and 2.5, and Ni concentrations in 100% sulfide (Ni tenor) ranging from 1 to 6 wt%, whereas the other Ni-rich class commonly has Ni/Cu greater than 3 and Ni tenor ranging from 6 to 36 wt%. In China, almost all Ni-Cu deposits belong to the Ni-poor class with low to moderate Ni tenor, such as the Jinchuan (Song et al., 2009), the Ni-Cu deposits occur at the Emeishan large igneous province (Baimazhai, Limahe and Yangliuping, Song et al., 2003; Wang et al., 2006; Tao et al., 2008), as well as the Ni-Cu deposits present in the Central Asian Orogenic Belt (CAOB), such as the Huangshandong, Huangshanxi, Kalatongke, Tianyu, Baishiquan, Hulu and Tulaergen deposits (Chai et al., 2008; Deng et al., 2014; Han et al., 2013; Li et al., 2012; Mao et al., 2008, 2015, 2014a,b; Qin et al., 2011; Song et al., 2013b; Tang et al., 2011; Xue et al., 2016; Yang et al., 2013b; Zhang et al., 2011; Zhou et al., 2004). On the other hand, the Huangshannan deposit in the Eastern Tianshan, southern CAOB, which is contemporaneous

* Corresponding authors at: Key Laboratory of Mineral Resources, Institute of Geology and Geophysics, Chinese Academy of Sciences, Beijing 100029, China (Y.-J. Mao, K.-Z. Qin).
Email addresses: maoyajing@mail.iggcas.ac.cn (Y-J Mao); kzq@mail.iggcas.ac.cn (K-Z Qin)

http://dx.doi.org/10.1016/j.oregeorev.2017.05.015
0169-1368/

with and has geochemical affinity with other magmatic Ni-Cu deposits in the CAOB (Mao et al., 2016; Zhao et al., 2015), is characterized by high Ni/Cu (mainly 2–8) and significantly higher Ni tenor (>10 wt%). It belongs to the Ni-rich class (Barnes and Lightfoot, 2005), which is different from other deposits in the CAOB.

Generally, high Ni tenor deposits are mainly associated with komatiitic and picritic magmas (Barnes and Lightfoot, 2005; Barnes et al., 2013), such as the Pechenga deposits of the Kola peninsula, Russia (Hanski et al., 2011), or the deposits of the East Yilgarn province (Barnes, 2006). The Ni content in sulfides related to komatiite is expected to be high since the parental magma is extremely rich in Ni as the result of high degree of mantle partial melting (Keays, 1995; Lesher and Keays, 2002), and Ni tenors in excess of 30% have been reported in unaltered komatiitic dunites (Barnes et al., 2011a). In addition, some of the high Ni tenor deposits have been interpreted as being related to hydrothermal process, as most of those deposits are associated with extensive alteration (Donaldson, 1981; Konnunaho et al., 2013; Sciortino et al., 2015). Undoubtedly primary high Ni tenor sulfides (>20%) related to high-Mg basalt parent magmas have been reported, in the Mirabela layered intrusion in Brazil (Barnes et al., 2011b) and in the Kevitsa deposit in Finland (Yang et al., 2013a). Previous studies of the Huangshannan deposit mainly focused on crustal contamination, source characteristics and magma emplacement (Zhao et al., 2015; Mao et al., 2016). Some uncertainties still exist, such as the cause of Pt and/or Pd anomalies (Pt and/or Pd depletion relative to other platinum group elements), the controlling factor of sulfide saturation and the origin of the high Ni tenor as well as possible exploration implications.

The technique of microbeam XRF mapping was used to estimate the Ni tenor of the Ni-rich sulfide component of the Huangshannan deposit deposits. The distribution of sulfide minerals in the XRF images, together with sulfide distribution in 3D at hand-sample scale, are used to constrain the cause of the Pt-Pd anomalies in sulfide-rich ores. The origin and deposition mechanism of these sulfides is evaluated based on whole-rock PGE geochemistry and Re-Os-S isotopes in sulfide separates, along with implications for the exploration potential for high Ni tenor sulfide in NW China.

2. Regional geology

The CAOB, situated between the Siberia craton to the north and the Tarim–Sino–Korean cratons to the south, is one of the largest accretionary arc and micro–continent collages of the Phanerozoic (Jahn, 2004; Xiao et al., 2009). The Eastern Tianshan and Beishan Terranes are located in the southern CAOB in NW China, (Fig. 1a). The Eastern Tianshan mainly consists of two tectonic units: Northern Tianshan (Bogeda–Haerlike belt and Jueluotage belt) in the north and Central Tianshan Massif in the south. The Northern Tianshan Terrane is made up of well developed Ordovician–Carboniferous volcanic rocks, granites and mafic–ultramafic complexes (BGMRXUAR, 1993). The Central Tianshan Massif is composed of the Precambrian crystalline basement (BGMRXUAR, 1993), and is bounded by the Aqikuduke–Shaquanzi Fault in the north and the Hongliuhe Fault in the south. The Beishan Terrane is located in the northeastern part of the Tarim Basin, adjacent to the Central Tianshan Massif in the north (Fig. 1b). It is mainly composed of the Precambrian crystalline basement and overlying sedimentary rocks, which encompass the Beishan, Gutongjing, Yangjibulake and Aierlanjigan groups (BGMRXUAR, 1993).

Mafic–ultramafic intrusive rocks associated with magmatic Ni-Cu deposits or occurrences formed during the amalgamation of continental blocks and terranes. They are widely distributed in the CAOB with large variation of age (430–216 Ma, Ao et al., 2010; Han et al., 2004, 2010; Qin et al., 2011; Song et al., 2013a; Su et al., 2011a; Sun et al., 2013a; Wu et al., 2004; Yang and Zhou, 2009). Most of the economic Ni-Cu deposits in CAOB are located in NW China and are

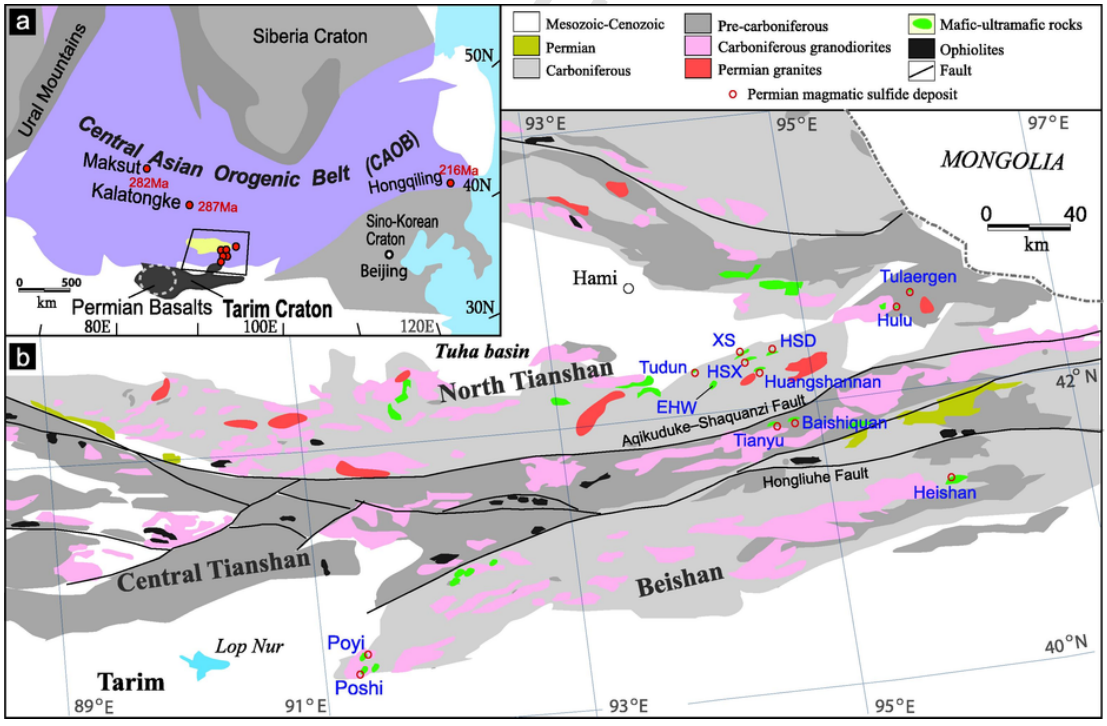

Fig. 1. Simplified geological map of the Central Asian Orogenic Belt (a, modified after Jahn, 2004) and the eastern Tianshan (b, modified from Xiao et al., 2004) showing the distribution of the mafic–ultramafic intrusions and associated magmatic sulfide deposits.

of Permian age (Fig. 1b) (Han et al., 2010; Qin et al., 2011; Su et al., 2011a; Sun et al., 2013a; Tang et al., 2011; Zhao et al., 2015). As shown in Fig. 1b, mafic–ultramafic intrusions with Ni–Cu sulfide mineralization are widely distributed in the Northern Tianshan, Central Tianshan Massif, and Beishan Terrane and the total Ni metal resource of these deposits reaches 1.5 million tons, using a cut-off grade of 0.3 wt% Ni (Mao et al., 2008). Specifically, economic Ni–Cu deposits in the Northern Tianshan include the Huangshandong, Huangshanxi, Huangshannan, Xiangshan, Tulaergen and Hulu intrusions with zircon U–Pb ages ranging between 274 Ma and 284 Ma (Han et al., 2004, 2010; Qin et al., 2011; Sun et al., 2013b). Tianyu and Baishiquan are Permian intrusions with sulfide mineralization located in the Central Tianshan (Tang et al., 2011). Permian mafic–ultramafic intrusions, such as the Poyi, Poshi, Hongshishan and Bijiashan intrusions are widespread in the Beishan Terrane, and most of those intrusions are characterized by low-grade Ni mineralization, high proportions of olivine, high Fo values, and high Ni contents in olivine (Qin et al., 2011; Su et al., 2011b; Xue et al., 2016). The Permian Kalatongke mafic intrusion with important Ni-Cu mineralization occurs in the north of NW China, 640 km from the intrusions in the Eastern Tianshan (Fig. 1a). This deposit differs from other deposits in its more Cu-rich sulfide composition and more evolved magma evident from a low proportion of olivine (Li et al., 2012; Qian et al., 2009; Song and Li, 2009; Zhang et al., 2009).

3. Geology of the Huangshannan intrusion

Drilling to date indicates that the Huangshannan deposit contains ~30 Mt of sulfide ores at 0.4 wt% Ni and 0.1 wt% Cu (Zhao et al., 2015). The sulfides are hosted within an elongated, lens-shaped, mafic–ultramafic intrusion emplaced into the Lower Carboniferous quartz schist (Wang et al., 1987). The intrusion is 5.2 km long and up to 1.3 km wide on the surface (Fig. 2a). The intrusion is composed of a tube-like ultramafic unit in the east and a lens shaped mafic unit in the central and west, and falls into the category of small magmatic conduits at transitions between vertical dikes and tubular sills or "chonoliths" (Barnes et al., 2016; Lightfoot and Evans-Lamswood, 2015). The east ultramafic unit consists of lherzolite, olivine websterite, and websterite, with lherzolite in the central grading into olivine websterite in the rim (Fig. 2a). The mafic unit, located in the central and western part of the intrusive complex, is composed of olivine gabbronorite, gabbronorite, leucogabbronorite and diorite (Fig. 2a and b) (Wang et al., 1987; Mao et al., 2016).

Potentially ore-grade Ni-Cu sulfide mineralization is present within the ultramafic unit, occurring as disseminated and net-textured ores. Commonly, high-grade mineralization occurs in the centers of the ore bodies, surrounded by low-grade ore (Fig. 2c). There are three main ore bodies in the ultramafic unit, the biggest two being located

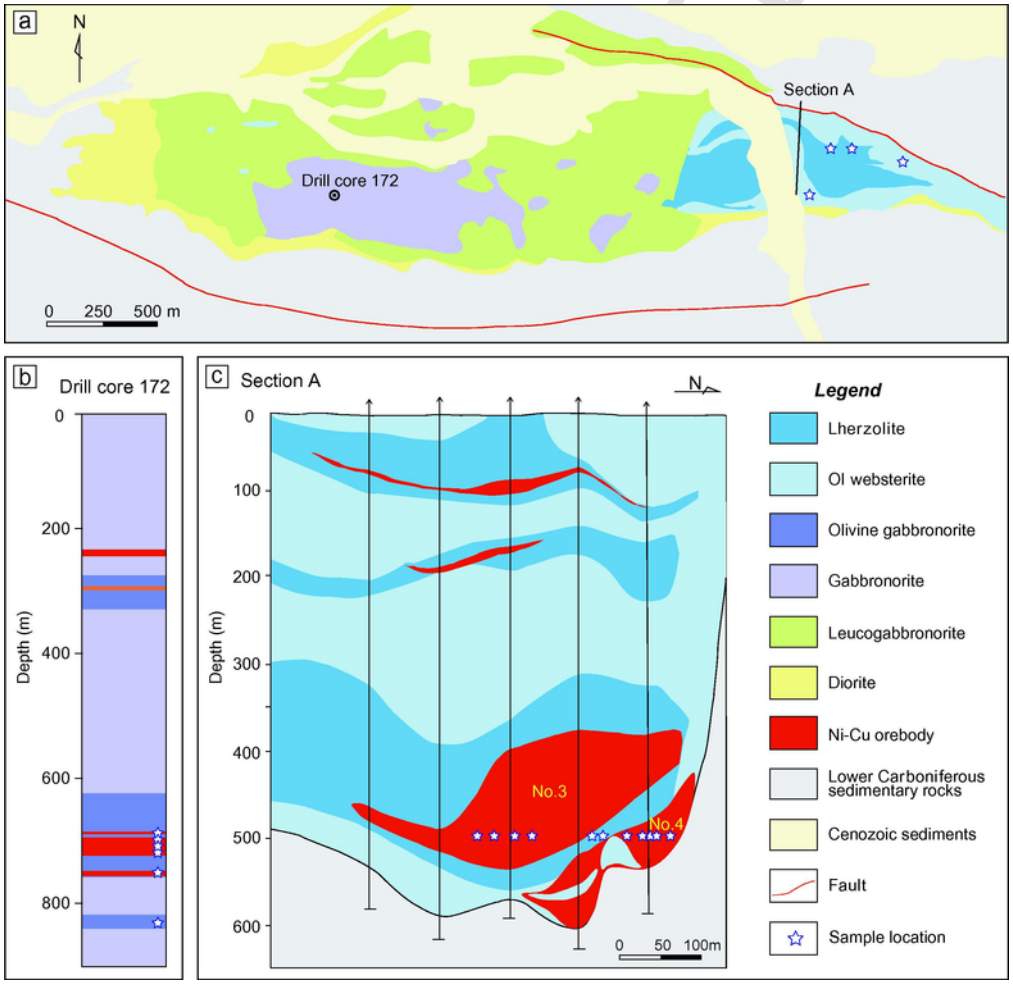

Fig. 2. Simplified geological map of the Huangshannan deposit, showing the distribution of Ni-rich disseminated ores in the ultramafic rocks and non-Ni-enriched Ni-Cu mineralization in the gabbronorite (After Wang et al., 1987 and exploration geological data).

near the bottom of the ultramafic unit (No. 3) and at the basal contact between the ultramafic unit and the wall rock (No. 4) (Fig. 2c). Ore body No. 3 is ~400 m long, 258 m wide, and ~120 m thick, containing 15 Mt sulfide ore at grades of 0.3 wt% Ni and 0.04 wt% Cu. Ore body No. 4 extends over 250 m length and 173 m width, with thickness up to 70 m, an average of 30 m, constituting ~4 Mt sulfide ore at Ni grade of 1.05 wt% and Cu grade of 0.29 wt% (from exploration geological data of 2015). Sulfide mineralization predominantly occurs as disseminated and net-textured assemblages, but minor massive and semi-massive ores are also present within the disseminated and net-textured sulfides as veins and their widths vary from few dm to 1 m. The massive and semi-massive ores also occur at the basal contact zone between the ultramafic unit and the wall rock schists. Although economic sulfide mineralization mainly occurs in the lherzolite and olivine websterite, disseminated sulfides are also present in the olivine gabbronorite. Exploration has been conducted in the mafic unit between 2014 and 2016. Disseminated sulfides have been found in a zone around 25 m thick within olivine gabbronorite in the lower part of the mafic unit.

Sulfide assemblages in lherzolite and olivine websterite are dominated by pentlandite, pyrrhotite, and chalcopyrite (Fig. 3, A1), similar to these in olivine gabbronorite. However, sulfides in lherzolite and olivine websterite are characterized by high proportions of pentlandite, whereas those in olivine gabbronorite are dominated by pyrrhotite.

4. Analytical methods

2D and 3D X-ray imaging were conducted at the CSIRO-Australian Resource Research Center (Perth). 2D petrographic images are combined with microbeam X-ray fluorescence elemental maps collected on a Bruker Tornado™ desktop instrument equipped with a rhodium target X-ray tube operating at 50 kV and 500 nA without filters and an XFlash® silicon drift X-ray detector, operating at a step size of 40 μm (pixel size) and a dwell time of 10 ms per pixel. The 3D distribution of the sulfides was determined using 3D X-ray Computed Tomography (XCT) data collected on a Medical X-ray CT scanning system (SOMATON Definition AS Medical CT Scanner). This instrument is composed of a rotating X-ray source producing a fan-shaped X-ray beam, along with a rotating set of X-ray detectors (Multislice UFC™ detectors), and a 100 kW generator. The X-ray source is fitted with a STRATON MX P High-Performance CT-X-ray tube, with intensity and voltage ranging from 20 to 800 mA and from 70 to 140 kV, allowing the X-ray to be transmitted through dense and complex material such as disseminated to blebby magmatic Fe-Ni-Cu sulfides. Reconstruction to produce the tomographic dataset was done on the Syngo® Acquisition Workspace and involves correction for anisotropic voxel sizes. The scanner was set up to 100 kV, 100 mA electron source, an Al–Cu filter, and a 0.38 rotation of the sample at each step (over 360°) allowing the collection of 1200 projections of the sample. Image reconstruction and processing were carried out using AvizoFire® (FEI) following a method similar to that described by Godel et al. (2010).

Rock samples for PGE analyses (hand sample, ~0.5 kg) were ground to <75 μm in size using an agate mill. The concentrations of PGE in sulfide-bearing samples were determined by the combination of NiS-bead pre-concentration, Te co-precipitation, and ICP-MS analysis in the National Research Center for Geo-Analysis, Beijing on 20 g sample aliquots. The concentrations of PGE in sulfide-poor samples were determined on 10 g aliquots by the Carius tube digestion and isotope dilution ICPMS technique of Qi et al. (2007) at the Institute of Geochemistry, Chinese Academy of Sciences in

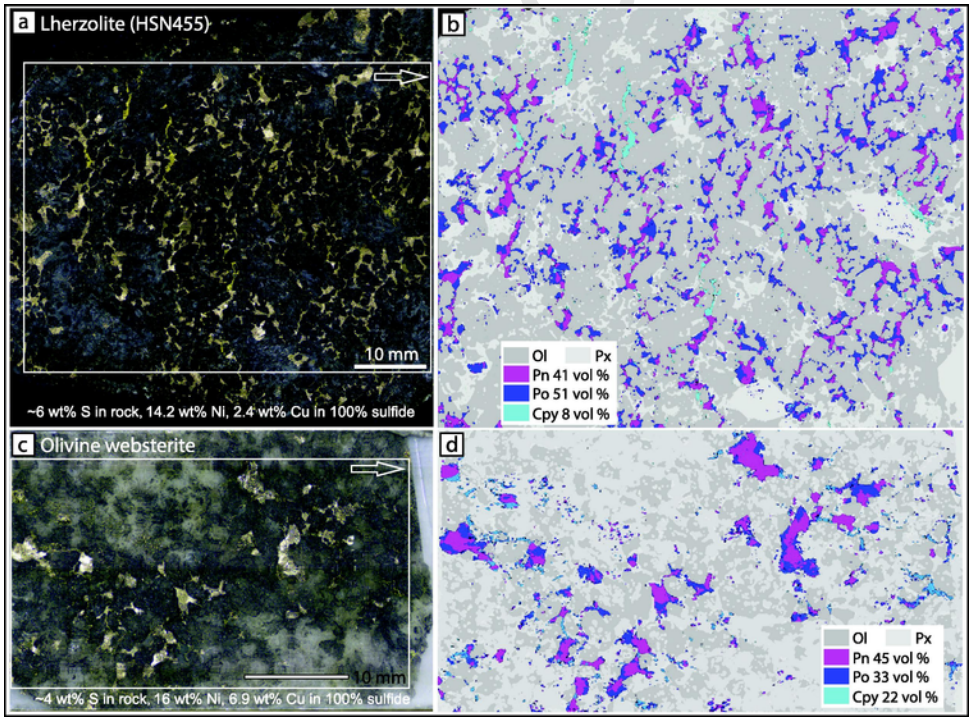

Fig. 3. Distribution of sulfide in lherzolite and olivine websterite. A, c: optical photomosaic of the cut surface; b, d microbeam XRF element distribution maps for areas indicated by rectangular boxes on a and c. Abundances are scaled to a maximum number of counts per element and shown as false-color three-channel RGB maps with Ni in the red channel, Cu in green, and S in blue. Cpy-chalcopyrite, Ol-olivine, Px-pyroxene, Pn-pentlandite, Po-pyrrhotite. (For interpretation of the references to colour in this figure legend, the reader is referred to the web version of this article.)

Guiyang. The detailed analytical procedures, blank concentrations, and detection limits are given in Qi et al. (2007). Sulfur concentrations in sulfide-poor rocks were determined using a LECO carbon–sulfur analyzer in the ALS Chemex laboratory, Guangzhou, China. In sulfide-bearing samples S, Ni, and Cu were analyzed by X-ray fluorescence in the same laboratory.

Sulfur isotope analyses were carried out at Indiana University (United States) using the continuous-flow method described in Studley et al. (2002). Coarse sulfide minerals such as pentlandite, chalcopyrite, and pyrrhotite were drilled from polished sections using a 0.75-mm carbide bit. Between 0.1 and 0.2 mg of sulfide powder was placed in tin cups with approximately 1.5–2 mg vanadium pentoxide (V_2O_5). Samples were prepared in an elemental analyzer by flash combustion at 1800 °C with a reactor column temperature of 1010 °C. Measurements of produced SO_2 were made using a Finnigan Delta V stable isotope ratio mass spectrometer, with results reported in per mil delta notation relative to Vienna Canyon Diablo Troilite (VCDT). Analytical uncertainty was less than ±0.05‰, and sample reproducibility was within ±0.2‰. Sulfide standards used were IAEA-S1, IAEA-S2, IAEA-S3, with values of −0.3, 21.7, and −31.3‰ respectively.

The chemical preparation and ICP-MS measurements of Re-Os isotopes were undertaken in the National Research Center of Geoanalysis (NRCG), Chinese Academy of Geological Sciences. Rhenium and Os concentrations were determined by isotope dilution. Detailed procedures for sample preparation are available in Du et al. (2004). Re and Os concentrations and isotopic compositions were measured by a PQ Excell ICPMS. ^{190}Os intensity was used to correct the interference of Os with Re and ^{185}Re intensity for Re with Os.

5. Results

5.1. Sulfide distribution and sulfide mineral proportion analysis

Sulfide distribution and textures are shown in the 2D and 3D images (Figs. 3 and 4). In 2D, most interstitial pentlandite and pyrrhotite are in contact and are connected with each other (Fig. 3b). Some of the chalcopyrites are distributed around the pentlandite and pyrrhotite, but most of the chalcopyrite is segregated at a scale of 2–5 mm (Fig. 3b and d). Pentlandite and chalcopyrite define a weak planar fabric (Fig. 3b). In 3D, the interstitial sulfide blebs in lherzolite (S content: ~5 wt%) form a 3D interconnected framework at decimeter scale (Fig. 4).

We determined mineral proportions by image-analysis work on the Tornado micro-XRF maps using ImageJ software, applying the method defined and described in Godel et al. (2007) based on the Backscattered Electron images. The proportion of pentlandite in sulfide from the disseminated ore varies from ~30 to >50 vol%, pyrrhotite from 30 to 60 vol% and chalcopyrite from 5 to 20 vol% (Table 1, Fig. 3b). Exceptionally, some olivine websterites have relatively high pentlandite and chalcopyrite proportion (Fig. 3c), e.g. 45 vol% and 22 wt% respectively (sample 15–4-7, Fig. 3c), on the scale of about 10 cm^2 of the sample surface.

Using the Ni/Fe ratios (1.12) of pentlandite obtained from scanning electron microscopic, the Fe/Ni atomic ratios in pentlandite can be calculated ($Fe_{4.36}Ni_{4.64}S_8$). Assuming that pyrrhotite has a Fe/S atomic ratio of 0.9 ($F_{0.9}S$) and that chalcopyrite has a stoichiometric Cu/Fe atomic ratio of 1 ($CuFeS_2$), the calculated Ni and Cu contents in 100% sulfides of ultramafic rocks vary from ~9 to ~19 wt% and from ~2 to ~7 wt%, respectively (Table 1).

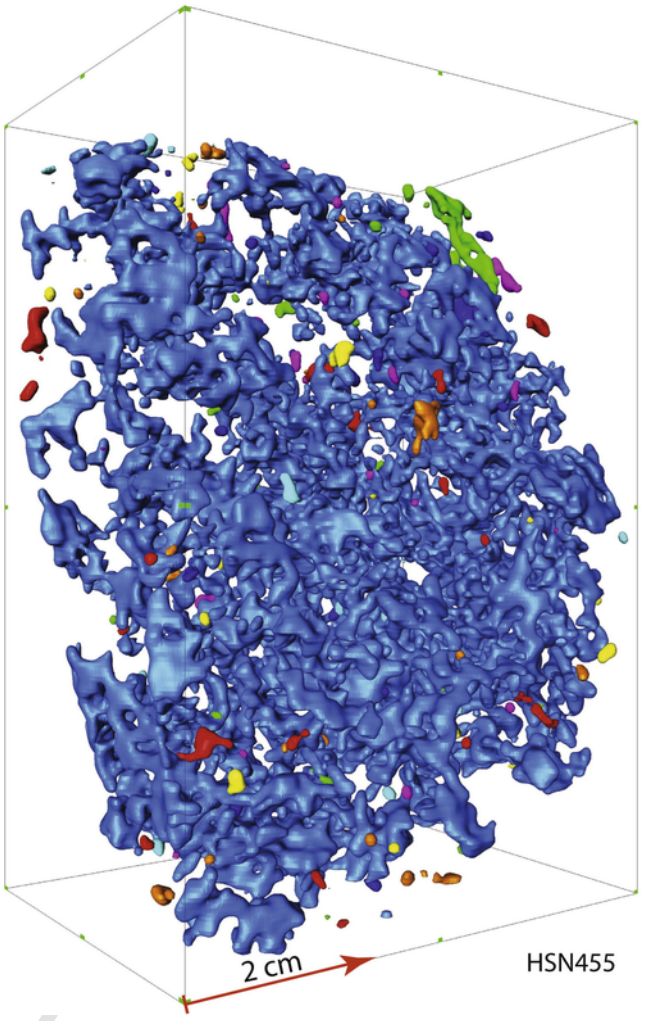

Fig. 4. 3D image of mineralized lherzolite based on the results of CT scans illustrating the distribution of disseminated sulfides in lherzolite with 5 wt% sulfur. Colors indicate individually connected frameworks of sulfide without compositional meanings. The blue object is a single interconnected framework of sulfide extending through the entire sample, showing that sulfides are well connected in disseminated ore which has S content of 5 wt%. (For interpretation of the references to colour in this figure legend, the reader is referred to the web version of this article.)

Table 1
Sulfide compositions estimated from XRF images.

Sample	Sulfide	Pn	Cpy	Po	Ni	Cu	Fe	S	Ni/Cu
	Vol%				wt%				
HSN455	13	41	8	51	14.2	2.4	45.9	36.0	6.0
14HSN35	14	40	5	55	14.0	1.6	46.8	36.2	8.9
14HSN36	17	28	8	64	9.7	2.4	49.9	36.9	4.0
14HSN37	14	32	7	61	11.1	2.3	48.8	36.6	4.9
14HSN16	4	57	13	30	19.7	4.0	39.6	35.5	5.0
15-4-5	6	44	9	47	15.3	2.7	44.6	36.3	5.6
15-4-6	6	32	17	52	11.1	5.2	46.3	36.6	2.1
15-4-7	9	45	22	33	16.0	6.9	40.4	35.2	2.3

Pentlandite (Pn), pyrrhotite (Po), and chalcopyrite (Cpy).

5.2. Whole rock S, Ni, Cu, PGE concentrations

Disseminated ore hosted in ultramafic samples from this study have sulfur concentrations between 4.7 wt% and 8.5 wt% (Table 2), slightly higher than those from Zhao et al. (2015), which have sulfur concentrations varying from 1 wt% to 3.6 wt%. Notably, Ni contents of disseminated ores hosted by ultramafic rocks are higher than those hosted by olivine gabbronorite and those hosted by ultramafic rocks from the Huangshandong, Huangshanxi, Tianyu, Poyi and Poshi deposits at same S content (Fig. A2a) (Mao et al., 2015, 2014a; Tang et al., 2011; Yang et al., 2013b; Zhang et al., 2009). Copper contents in the ultramafic rocks overlap with those in the other deposits (Fig. A2b). We use the equation of Barnes and Lightfoot (2005) to back calculate the 100% sulfide composition. We only use samples contain >2 wt% S of the Huangshannan deposit to eliminate the uncertainty generated by back calculation, within the range of reliability determined by Barnes et al. (2011b). In addition, the contributions of Ni from olivine were corrected using the average Ni contents in olivine of 3000 ppm (Mao et al., 2016), which is close to the upper limit of the Ni content in olivine, and assuming the lherzolite and olivine websterite samples contain olivine of 70 vol% and 40 vol%, respectively. In the plot of Ni versus Cu in 100% sulfide (Fig. 5), the sulfide fraction in the ultramafic rocks has high Ni tenor (9–19 wt%) and medium Cu tenor (1–7 wt%), in good agreement with estimates from XRF mapping and image analysis, whereas sulfide in olivine gabbronorite has relatively low Ni (~5 wt%) and Cu (~2 wt%) tenors. The Ni [illegible] of the ultramafic rocks from the Huangshannan deposit is similar [illegible] Xiarihamu Ni-rich ore (Song et al., 2016) but significantly higher than other deposits in NW China, whereas Cu tenor is slightly lower than those of the other deposits (Fig. 5).

Good correlations between S and Os, Ir, Ru, and Rh are observed for ultramafic rocks, except for samples with >10 wt% S (Fig. A3a–d), whereas the correlations between S and Pt and Pd are relatively poor (Fig. A3e and f). Samples with sulfur contents greater than 4.5 wt% have relatively low Cu (Fig. A2b), Pt, and Pd tenors, defined as concentrations in 100% sulfide (Fig. A3e and f). The mantle normalized tenors of these samples exhibit significant Pt and/or Pd depletion relative to other PGEs (Fig. 6a), which is also shown in sulfide-rich samples from the Tianyu and Huangshanxi deposits (Tang et al., 2011; Mao et al., 2014a,b). A strong positive correlation between Os and Ir is shown in sulfides from the Huangshannan deposit (Fig. 7a), and a positive correlation is also present between Ir and Pd, for sulfides without Pt and Pd depletion (Fig. 7b). Sulfide-rich samples (S > 4.5 wt%) tend to have lower Cu, Pt, and Pd tenors than sulfide-poor samples (Fig. 8). Nickel tenor in 100% sulfides is positively correlated with Os and Ir tenors (Fig. 9).

5.3. Sulfur and Re-Os isotopes in sulfide

The $\delta^{34}S$ values of pyrrhotite, pentlandite, and chalcopyrite in lherzolite and olivine gabbronorite range from −0.4 to 0.8‰ (Table 3), similar to typical mantle values. There is no sulfur isotope data available for the wall rocks of the Huangshannan intrusion. However, previous studies of nearby deposits indicate that the Carboniferous rocks regionally have variable $\delta^{34}S$ values, ranging from 1.3 to 7.2‰ around the Xiangshan deposit, and ranging from 1.8 to 3.4‰ around the Tulaergen deposit (Tang et al., 2012). Sulfides from most magmatic Ni-Cu sulfide deposits in NW China, such as the Huangshandong, Huangshanxi and Kalatongke deposits (Qian et al., 2009; Wang et al., 1987) are dominated by mantle like $\delta^{34}S$ values, but variations of the $\delta^{34}S$ values of those deposits are wider than at the Huangshannan deposit (Fig. 10).

The Re tenors in the separated sulfides from lherzolite vary from 156 to 196 ppb, whereas those from olivine websterite and olivine gabbronorite vary from 71 to 76, 220 to 244 ppb respectively (Table 4). The Re/Os of sulfides from lherzolite vary from 4.9 to 6.8, whereas those in olivine websterite and olivine gabbronorite vary from 0.7 to 19 and from 7.3 to 20, respectively. $^{187}Os/^{188}Os_i$ and γOs (at 278 Ma) of lherzolite and olivine websterite vary from 0.27 to 0.29 and from 108 to 129 respectively, whereas those of olivine gabbronorite vary from 0.27 to 0.37 and from 113 to 188 respectively. Re-Os isotope data exhibit a large spread in $^{187}Re/^{188}Os$ (3.6–97) and define an isochron with an age of 299.5 ± 10 Ma, which is slightly older than the zircon U-Pb ages (278 ± 2 Ma, Mao et al., 2016) from the magmatic system. Overall, the range of variation of $^{187}Os/^{188}Os_i$ and γOs values of samples from the Huangshannan intrusion is relatively narrow ($^{187}Os/^{188}Os_i$ of 0.27–0.29, γOs of 108–129) except for one gabbronorite sample ($^{187}Os/^{188}Os_i$ of 0.37, γOs of 188). There is no positive correlation between γOs values and Re/Os (Fig. 11a), which is a different result from observed at the Poyi and Poshi deposits regionally (Yang et al., 2013b). In addition, the γOs values of the sulfide of the Huangshannan deposit (108–188) are significantly higher than the depleted mantle reservoir which has been estimated at −3.1 to −0.8 at the time of formation of the deposit (Shirey and Walker, 1998).

Table 2
Sulfur, Ni, Cu and PGE concentrations in whole rocks from the Huangshannan deposit.

No.	Sample	Rock Type	S	Ni	Cu	Co	Os	Ir	Ru	Rh	Pt	Pd
			wt.%				ppb					
1	ZK172-1-823	Ol gabbronorite	0.10	0.05	0.01	0.01	0.07	bdl	bdl	bdl	bdl	bdl
2	ZK172-1-695	Ol gabbronorite	0.83	0.12	0.04	na	0.28	0.14	0.18	0.16	8.69	0.96
3	ZK172-1-720	Ol gabbronorite	2.07	0.22	0.07	na	1.16	0.55	0.91	0.51	36.30	1.76
4	ZK172-1-768.5	Ol gabbronorite	2.81	0.35	0.16	na	0.93	0.40	0.63	0.46	21.40	0.44
5	HSN12	Ol websterite	0.19	0.09	0.01	0.01	0.09	bdl	bdl	bdl	bdl	bdl
6	HSN12-1	Ol websterite	0.18	0.09	0.01	0.01	0.08	bdl	bdl	bdl	bdl	bdl
7	ZK2605-36	Lherzolite	0.22	0.20	0.01	0.01	0.17	bdl	bdl	bdl	bdl	bdl
8	ZK1701-257	Lherzolite	0.47	0.23	0.06	0.01	0.29	bdl	bdl	bdl	bdl	0.28
9	ZK42-1-86	Lherzolite	0.11	0.21	0.01	0.01	0.93	0.03	0.06	0.06	0.79	0.47
10	HSN455-1	Lherzolite	8.85	3.81	0.55	0.06	10.40	3.93	5.69	4.09	2.51	40.00
11	HSN455-2	Lherzolite	4.73	2.30	0.25	0.04	5.77	2.64	3.55	2.36	5.02	2.20
12	HSN455-5	Lherzolite	5.34	2.56	0.29	0.04	5.68	2.35	3.33	2.09	4.78	3.35
13	HSN455-6	Lherzolite	6.77	3.13	0.76	0.05	6.06	2.57	3.55	2.78	4.13	26.00

na-not analyzed, bdl-below detection limit.

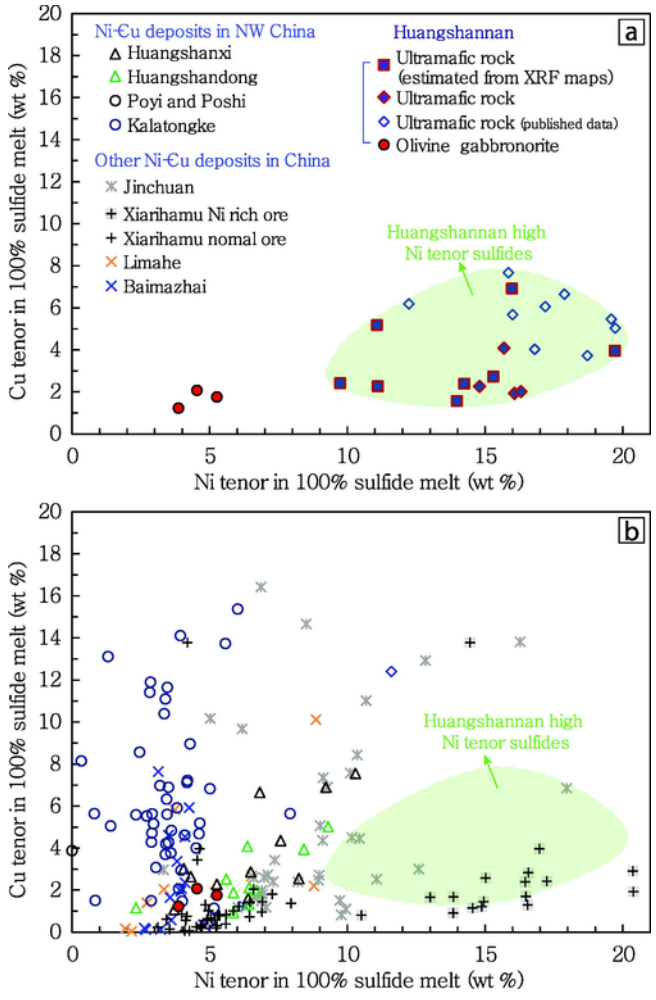

Fig. 5. Plot of Ni versus Cu content in recalculated 100% sulfide for rocks from the Huangshannan deposit (a) and comparison with other deposits in China (b). Data source: Baimazhai (Wang et al., 2006), Huangshannan deposit (this study, Zhao et al., 2015), Huangshandong (Gao et al., 2013; Mao et al., 2015), Huangshanxi (Mao et al., 2014a; Zhang et al., 2011), Jinchuan (Chai and Naldrett, 1992; Song et al., 2009), Kalatongke (Song and Li, 2009), Limahe (Tao et al., 2008), Poyi and Poshi deposits (Yang et al., 2013b), Xiarihamu deposit (Li et al., 2015; Song et al., 2016).

6. Discussion

6.1. Pt and Pd depletion in sulfide-rich samples

Significant Pt and/or Pd anomalies, in the form of Pt depletion and moderate Pd depletion relative to other PGEs, are commonly present in sulfur-rich samples (Fig. 6a) in NW China, such as the Huangshannan (S > 4.5 wt%), Tianyu (S > 9 wt%) and Huangshanxi (S > 12 wt%). Previous studies attributed these to hydrothermal alteration (Mao et al., 2014a; Tang et al., 2011) as PPGE are more mobile than IPGE in hydrothermal fluids. However, the interpretation does not seem applicable for the Huangshannan deposit, at least not for the lherzolites, which show little sign of alteration (Fig. 3a and b). Pd is commonly more soluble than Pt in most fluids (Barnes and Liu, 2012), thus hydrothermal processes tend to produce a scatter of Pd concentrations compared to Pt. Le Vaillant et al. (2016) investigated PGE behavior during low-temperature hydrous alteration of disseminated Ni-Cu-(PGE) ores of the Kevitsa deposit, and found no evidence of mobility for either Pt or Pd.

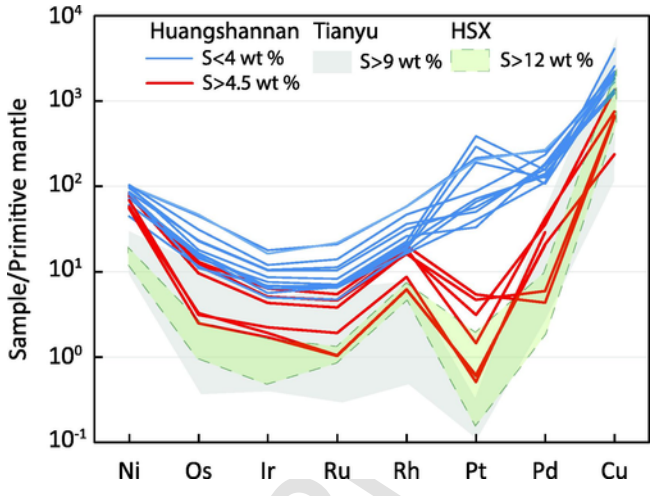

Fig. 6. Mantle-normalized plots for 100% sulfide from the Huangshannan deposit, showing sulfide rich ores (>4.5 wt%) are generally depleted in Pt and Pd. Similar PGE distribution patterns occur at sulfide rich ores from the Huangshanxi (S > 12 wt%) and Tianyu (S > 9 wt%) deposits. The primitive mantle values are from Barnes and Maier (1999).

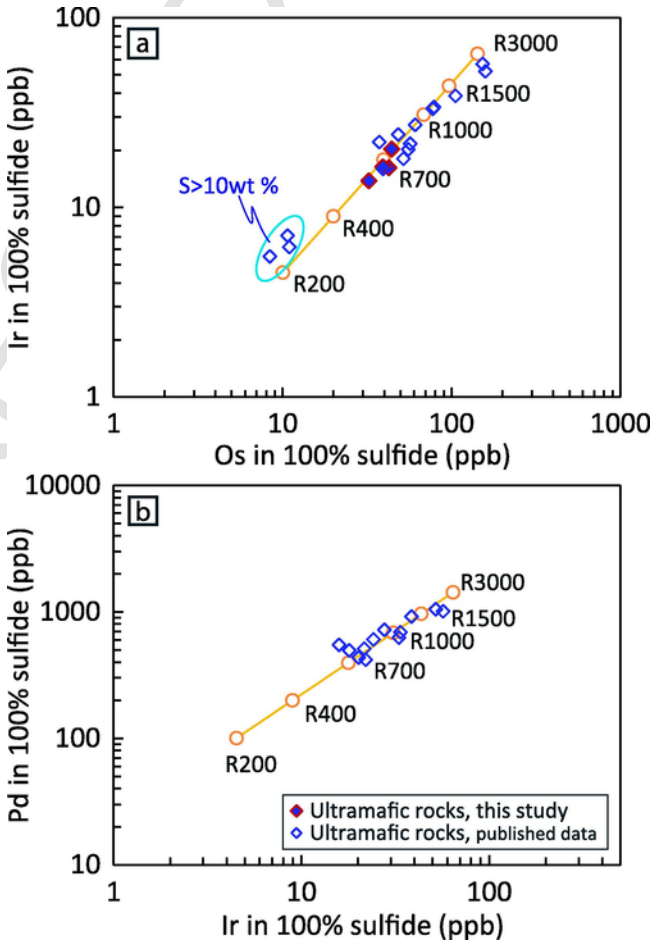

Fig. 7. Plots of Os versus Ir (a), Pd (b) and Ir versus Pd (c) contents in recalculated 100% sulfide for samples with >1 wt% S from the Huangshannan deposit, compared with model curves for constant starting silicate composition given in the text, and D_{Os}, D_{Ir} and D_{Pd} values of 300,000 (Mungall and Brenan, 2014). Data source is the same to these listed in Fig. 5.

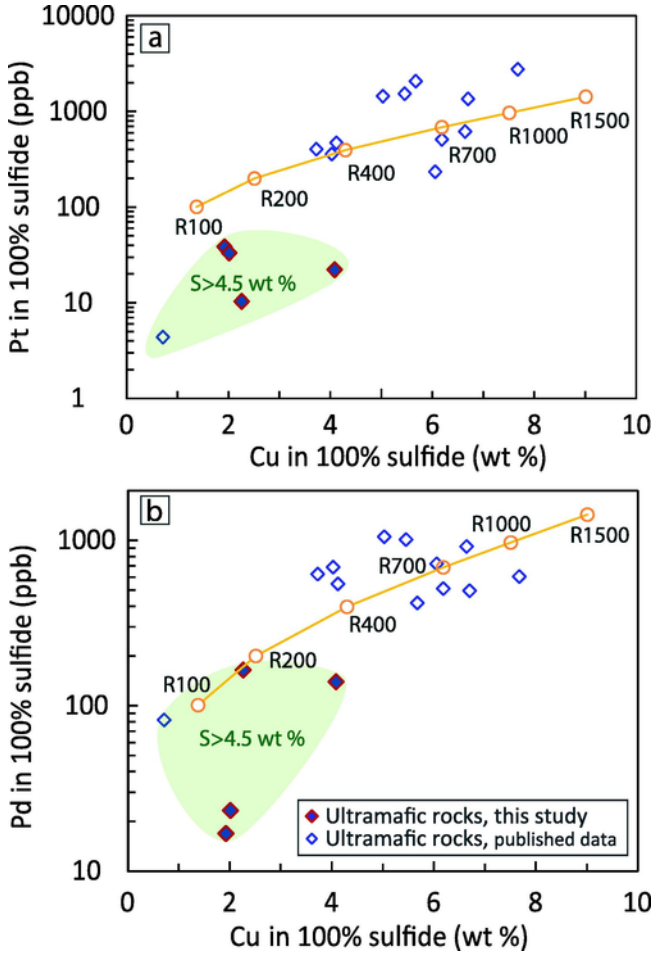

Fig. 8. Plot of Cu versus Pt (a) and Pd (b) contents in recalculated 100% sulfide from the Huangshannan deposit. It is shown that samples with lower Cu tenors also have relatively lower Pt and Pd tenors.

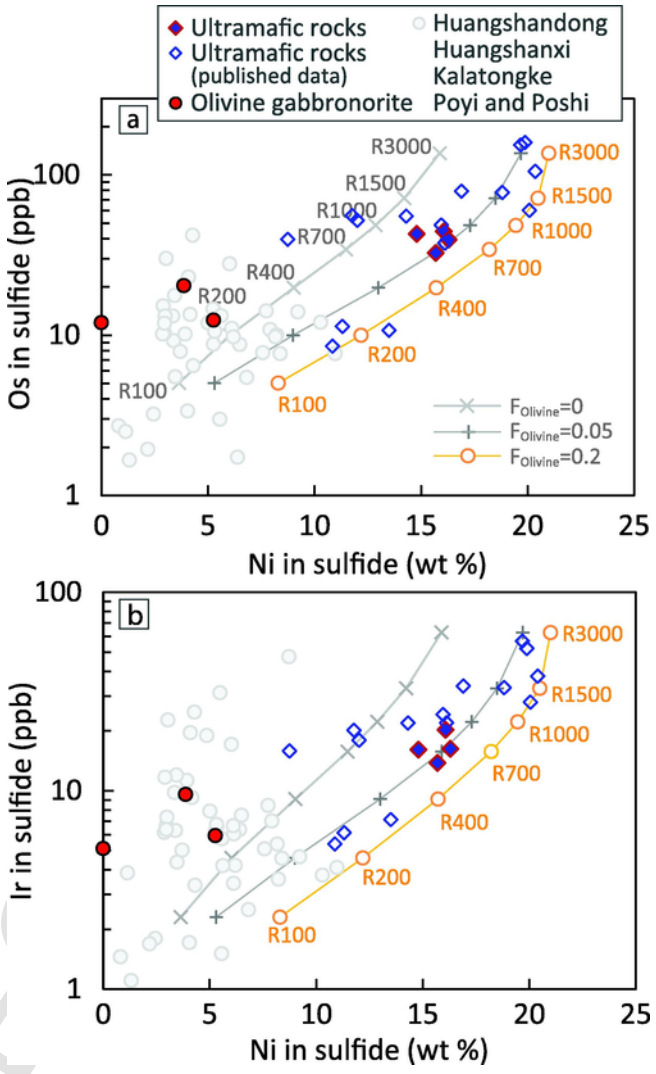

Fig. 9. Sulfide composition of the Huangshannan deposit, expressed as Ni versus Os (a) and Ir (b), compared with model curves for various R value and different olivine content in the system. F_{Ol} indicates the mass ratio of olivine to silicate melt. The start composition and modeling results are given in Table 5.

On the other hand, the Pt-Pd anomalies in sulfide-rich samples could be the result of monosulfide solid solution (MSS) fractionation from sulfide liquid during cooling, similar to the compositional zoning shown in the sulfide orebodies at the Sudbury and Noril'sk nickel camps (Naldrett et al., 1997, 1982), as Pt and Pd are incompatible in early crystallizing MSS and hence become enriched in Cu-rich residual sulfide melt (Barnes and Lightfoot, 2005). This mechanism is well established in massive sulfide ores but is more difficult to apply in the case of disseminated ores, owing to the difficulty of separating the residual Cu-enriched liquid from the solid MSS crystals. However, where interstitial sulfides form an interconnecting framework, the negative buoyancy of the connected sulfide could force the sulfides to percolate down through the intercumulus pore space during or after MSS crystallization (Barnes et al., 2017; Chung and Mungall, 2009), even where sulfide abundance is as low as 5%. Interconnected residual sulfide liquid may continue to percolate to the bottom of the ore zone and even to the wall rock to form Cu-rich sulfides (Mungall, 2002), leaving solid MSS behind. This explanation is consistent with the relatively low Cu tenor of sulfide-rich samples (Fig. 8a and b). This is also supported by the textural evidence reported above that chalcopyrite forms a continuous network at decimeter scale (Fig. 3a and b), and by the fact that almost all sulfides are interconnected with each other in the 3D model of samples with as little as ~6 wt% sulfur (Fig. 4). From these observations, we deduce that MSS fractionation, together with the percolation of

Table 3
Sulfur isotopes of sulfides from the Huangshannan deposit.

Sample	13 HSN-2	13 HSN-2	13 HSN-3	13 HSN-6	13 HSN-6	HSN455-1	HSN455-2	HSN455-3	172–798.5	172–798.5	172–695	172–720
Rock type	Lherzolite	Lherzolite	Lherzolite	Lherzolite	Lherzolite	Lherzolite	Lherzolite	Lherzolite	Ol gabbronorite	Ol gabbronorite	Ol gabbronorite	Ol gabbronorit
Mineral	Po	Cp	Po	Cp	Pn	Po	Po	Po	Po	Po + Pn	Po + Pn	Po + Pn
$\delta^{34}S/^{32}S$	0.6	0.4	0.8	0.8	0.4	0.6	0.5	0.5	0.5	−0.3	0.1	−0.4

Po-pyrrhotite, Pn-pentlandite, Cpy-chalcopyrite.

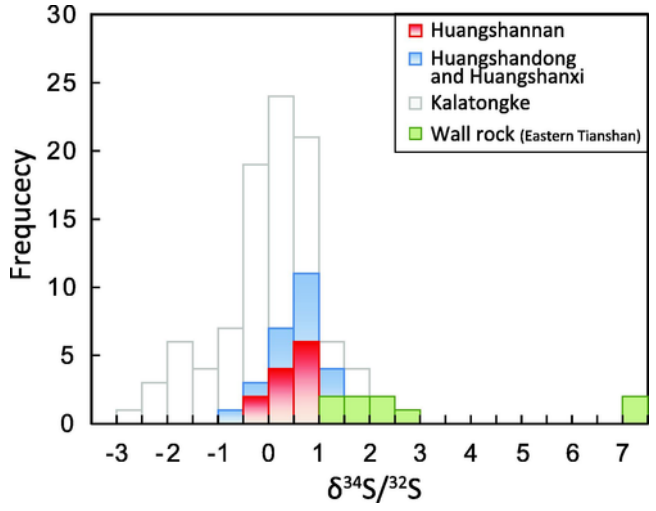

Fig. 10. Sulfur (^{34}S) isotopic composition of the Huangshannan deposit and comparison with other deposits in NW China. Data source: Huangshannan (this study), Huangshandong and Huangshanxi deposits (Wang et al., 1987), Kalatongke deposit (Wang and Zhao, 1991), wall rocks in the Eastern Tianshan (Tang et al., 2012).

Cu-rich sulfides, is the main explanation for the observed Pt and Pd depletions in the sulfide-rich samples in the Huangshannan intrusion. This finding suggests that post modification may not be necessary to account for Pt and/or Pd anomalies in sulfide-rich ores regionally.

A further distinctive feature of the Huangshannan S-rich ores is a marked depletion of Pt over Pd, a feature noted in many examples of massive sulfide ores from a variety of ore types including komatiites (e.g. Barnes et al., 1988), to date unexplained. The presence of complementary positive Pt anomalies in some of the S-poor ores suggests that Pt may be fractionated from Pd during the coupled percolation-differentiation process by the crystallization of solid Pt phases and retention as part of the cumulate sulfide assemblage left behind in the silicate cumulate pile as the sulfide liquid drains. This cannot be the complete explanation, as the S-rich ores are depleted in all PGEs relative to the disseminated ores implying that they are part of a separate batch of low R sulfides, but they may still be the result of accumulation of percolating melt that had lost Pt by this mechanism.

6.2. Origin of the high Ni tenor sulfides

The high Ni tenor samples from the Huangshannan deposit are fresh and show no evidence for major hydrothermal modification, indicating a magmatic origin rather than modification by hydrothermal alteration processes. High Ni tenor deposits with magmatic origin have been reported in previous studies (Barnes et al., 2013, 2011a; Yang et al., 2013a), and the controlling factor in forming high Ni tenor deposits are attributed to the following two aspects: 1) sulfide equilibrium with silicate melt, with or without additional olivine, at high R values (Barnes et al., 2013, 2011a) (R value represents mass ratio of silicate to sulfide liquid, Campbell and Naldrett, 1979), 2) derivation from unusually Ni-rich parental magmas, such as komatiites, or magmas derived from pyroxenite mantle sources (Sobolev et al., 2007) (still requiring high R values), or 3) addition of external Ni by assimilation of pre-existing Ni-enriched rocks (Yang et al., 2013a).

During equilibrium of sulfide, olivine, and silicate melt, equilibration between sulfide liquid and olivine is expressed in terms of the exchange coefficient for Fe and Ni, $K_D = (X_{NiS}/X_{FeS})_{sulfide\ liquid}/(X_{NiO}/X_{FeO})_{olivine}$ (Brenan and Caciagli, 2000). The positive dependence of K_D on Ni + Cu content of sulfide liquid, as well as on fO_2, has been demonstrated experimentally and gives rise to a critical nonlinearity in the relationship between sulfide and olivine-saturated silicate liquid compositions (Barnes et al., 2013). Firstly, we have used the equation of Barnes et al. (2013) to estimate the oxidation state for the Huangshannan magmatic sulfide deposit based on four lherzolite samples with disseminated ore; olivine compositions of those samples are given in Mao et al. (2016). As shown in Fig. 12a, the estimated oxidation state for the Huangshannan deposit is close to QFM + 0.5 (i.e., fO_2 0.5 log unit higher than the value for the quartz–fayalite–magnetite buffer), similar to those from the Mirabela high Ni tenor deposit (Barnes et al., 2013), as well as the Jinchuan deposit (Chai and Naldrett, 1992). Then, the sulfide-olivine-silicate melt equilibria of the Huangshannan deposit was modeled using the calculation procedure by Barnes et al. (2013). Input parameters including magma composition, olivine composition, D_{Ni} and K_D are presented in Table 5 along with the modeling results. As shown in Fig. 12b, most of the sulfide tenors of the ultramafic rocks are consistent with sulfide-silicate melt equilibrium at high R values (>600) or sul-

Table 4
Rhenium and Os concentrations and Os isotope ratios of pyrrhotite and pentlandite from the Huangshannan deposit.

No.	Sample	Rock type	Mineralization	Mineral	wRe	σ	wOs	σ	$w^{187}Os$	σ	$^{187}Re/^{188}Os$	σ	$^{187}Os/^{188}Os$	σ	Re/Os	$(^{187}Os/^{188}Os)i$
					ppb		ppb		ppb							
1	HSN455-4	Lherzolite	Disseminated	Po	162.1	1.2	33.0	0.4	1.626	0.02	23.77	0.31	0.3793	0.0040	4.9	0.27
2	HSN455-7	Lherzolite	Disseminated	Po	191.5	1.5	28.3	0.3	1.598	0.02	32.69	0.41	0.4342	0.0040	6.8	0.28
3	HSN455-2 (pn)	Lherzolite	Disseminated	Pn	155.9	1.1	29.0	0.3	1.469	0.01	25.98	0.30	0.3897	0.0028	5.4	0.27
4	HSN455-1 (pn)	Lherzolite	Disseminated	Pn	196.0	1.5	30.0	0.4	1.664	0.02	31.53	0.47	0.4259	0.0064	6.5	0.28
5	HSN19-4 (pn)	Olivine websterite	Disseminated	Pn	70.9	0.5	95.6	0.8	3.562	0.03	3.58	0.04	0.2863	0.0015	0.7	0.27
6	HSN19-4	Olivine websterite	Disseminated	Po	75.6	0.6	3.9	0	0.372	0	93.06	1.06	0.7282	0.0056	19.3	0.29
7	ZK172-1-720	Olivine gabbronorite	Disseminated	Pn	220.1	1.7	20.9	0.2	1.649	0.01	50.91	0.56	0.6068	0.0027	10.5	0.37
8	ZK172-1-606	Olivine gabbronorite	Disseminated	Pn	243.6	2	33.6	0.5	1.908	0.03	35.01	0.61	0.4363	0.0079	7.3	0.27
9	ZK172-1-768.5	Olivine gabbronorite	Disseminated	Pn	221.8	1.7	11.0	0.1	1.064	0.01	97.33	1.33	0.7427	0.0089	20.1	0.29

Po-pyrrhotite, Pn-pentlandite, γOs calculated as defined by Shirey and Walker (1998), t = 278 (Mao et al., 2016).

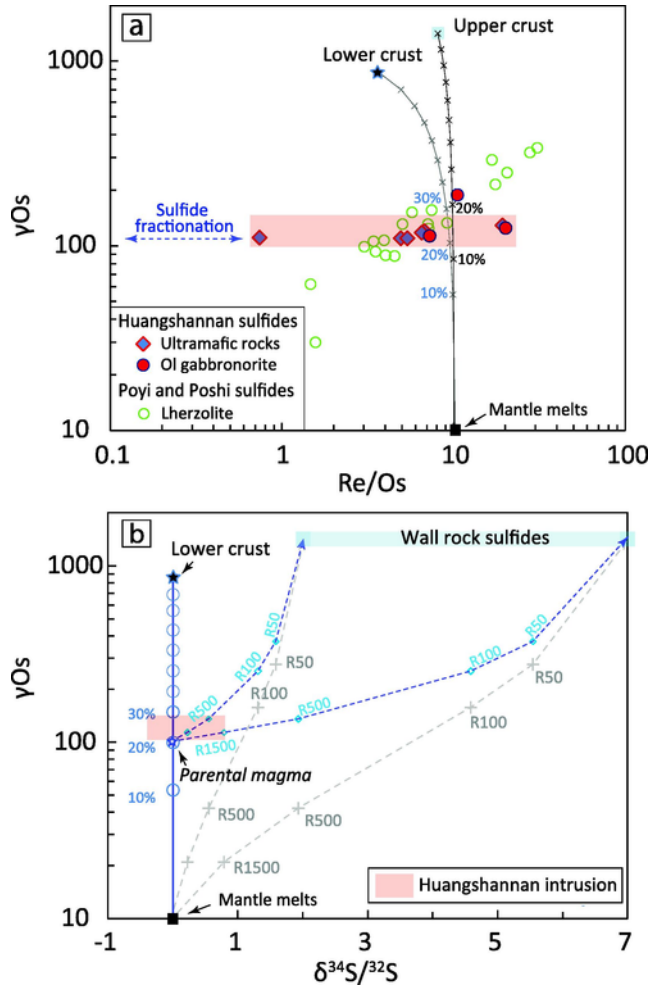

Fig. 11. Plot of γOs versus Re/Os ratios (a) and $\delta^{34}S/^{32}S$ (b) for sulfide separates from the Huangshannan deposit and comparison with sulfide from the Poyi and Poshi deposits. The gray lines in (a) represent bulk mixing of mantle melts with lower crust and upper crust materials. Modeling lines in (b): the blue line with circles represents isotopic variation during stage 1 contamination between mantle melts and bulk lower crust. Dashed blue lines represent stage 2 contamination between pre-contaminated mantle melt and wall rock sulfides at variable R values. Dashed gray lines show the isotopic variations of the mantle melt when contaminated by wall rock sulfides at viable R values. Modeling results indicate that about 20 wt% crustal material addition into the mantle-derived melt plus wall rock sulfide assimilation at high R value circumstance can give rise to the Os-S isotopic compositions of the Huangshannan deposit. (Os = 0.1 ppb, $^{187}Os/^{188}Os_i = 0.14$, $\delta^{34}S = 0‰$) Shirey and Walker, 1998, Os = 0.05 ppb, $^{187}Os/^{188}Os_i = 1.93$ at 278 Ma, Os = 0.1 ppb, $^{187}Os/^{188}Os_i = 0.8$ at 278 Ma, $\delta^{34}S = 0‰$ similar to these proposed by (, wall rock sulfide (Os = 1.2 ppb, $^{187}Os/^{188}Os_i = 1.93$ at 278 Ma, $\delta^{34}S = 1.9–7.2‰$) (Tang et al., 2011; Yang et al., 2013b). (For interpretation of the references to colour in this figure legend, the reader is referred to the web version of this article.)

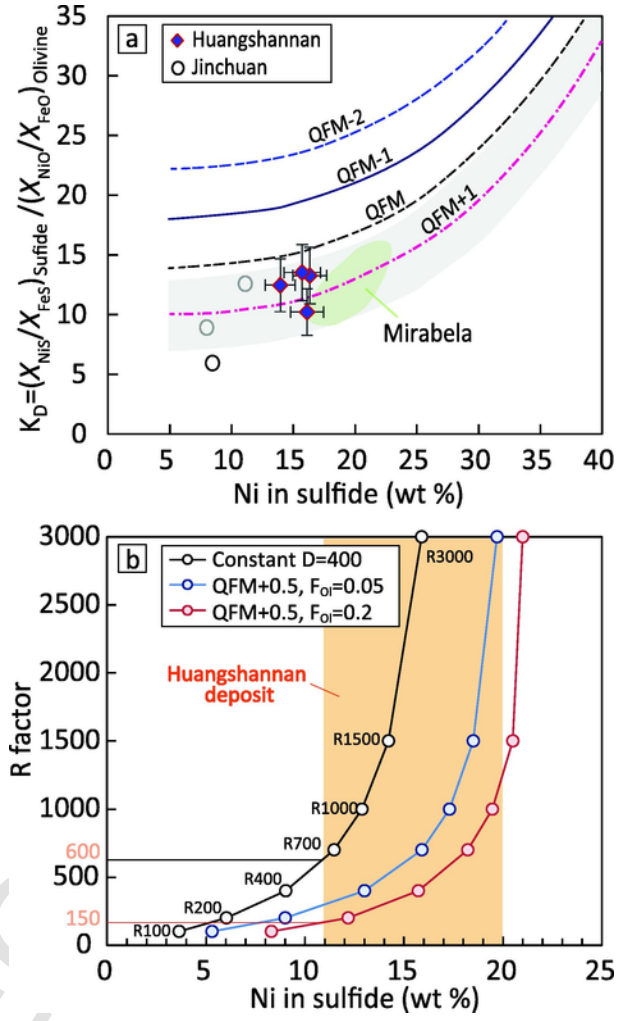

Fig. 12. The oxidation state of the Huangshannan magmatic sulfide deposit determined using olivine compositions and Ni contents in bulk sulfide (a), Ni tenor versus R factor modeling compared with model curves for various R value and different olivine content in the system. F_{Ol} indicates the mass ratio of olivine to silicate melt. Olivine composition of the sulfide mineralized lherzolite is given in Mao et al. (2016). The base of the plot and the results for Jinchuan and Mirabela deposits are from Barnes et al. (2013).

fide-silicate-olivine equilibrium at moderate R-value (>150) for initial olivine content between 5% and 20%. However, sulfide with Ni tenor higher than 16 wt% cannot be generated from sulfide equilibrium without the presence of olivine in the initial phase assemblage (Fig. 12b).

The incorporation of olivine into the mass balance equation accounts for an additional 3–5 wt% Ni in sulfide for the Huangshannan deposit, compared with equilibration between silicate and sulfide liquid in the absence of olivine. In addition, Ni contents in olivine from sulfide-bearing samples and from sulfide-poor samples are identical (Fig. 13), consistent with equilibrium at high R values. On the other hand, high Ni tenor of the Huangshannan deposit would also be consistent with the R modeling alone if the parental magma had Ni as high as ~600 ppm, but it is not consistent with the previous estimate of ~450 ppm Ni (Mao et al., 2016). It is important to note that the high Ni contents in the olivine of the Huangshannan deposit (Fig. 13) are slightly higher for the same Fo content than the Ni-rich olivine phenocrysts found in Ni-rich magma derived from pyroxenite source and emplaced over thick lithosphere (OIB and LIP, >70 km thick) (Sobolev et al., 2007). This observation strongly suggests that the Huangshannan parental magma is relatively rich in Ni.

6.3. Modeling of PGE concentrations in the parental magma and deposition of the sulfide liquid

We carried out R factor modeling for samples from the Huangshannan deposit to better constrain the key factors in controlling the primary composition of the sulfide melt in ultramafic rocks during sulfide segregation. In the modeling, Ni content in the Huangshannan parental magma of 450 ppm is used (Mao et al., 2016), D_{PGE} and D_{Ni} between sulfide and silicate melt are assumed as 300,000 and 400

Table 5
Start magma composition and results of model calculation.

Magma composition					
fO_2	MgO (wt.%)	FeO (wt.%)	Ni (ppm)	Dni(sul-sil)	
QFM 0.5	12.4	10	450	400	
Result K_D					
F ol*	R factor	K_D	Ni in sulfide	Ni in olivine	Fo in olivine
0	100	/	3.6	/	/
0	200	/	6.0	/	/
0	400	/	9.0	/	/
0	700	/	11.5	/	/
0	1000	/	12.9	/	/
0	1500	/	14.2	/	/
0	3000	/	15.9	/	/
0.05	100	9.9	5.3	1060	87.4
0.05	200	10.2	9.0	1767	87.4
0.05	400	10.8	13.0	2486	87.4
0.05	700	11.5	15.9	2988	87.4
0.05	1000	12.0	17.3	3254	87.4
0.05	1500	12.5	19.0	3497	87.4
0.05	3000	14.7	19.7	3700	87.4
0.2	100	12.1	8.8	1423	87.4
0.2	200	12.7	13.2	2223	87.4
0.2	400	13.7	16.9	2843	87.4
0.2	700	14.5	19.2	3268	87.4
0.2	1000	14.8	20.0	3481	87.4
0.2	1500	15.0	20.4	3670	87.4
0.2	3000	15.2	21.0	3889	87.4

* F_{Ol}-mass ratio of olivine to silicate melt, $K_D = (X_{NiS}/X_{FeS})_{sulfide\ liquid}/(X_{NiO}/X_{FeO})_{olivine}$.

(Mungall and Brenan, 2014), respectively. Samples with less than 1 wt% S are excluded from the modeling as the error in extrapolation to 100% sulfide composition calculation becomes prohibitively large (Barnes et al., 2011b), and the samples which have experienced Cu-rich residual sulfide melt percolation are included for the Os versus Ir modeling, but excluded for the modeling of Ir and Os versus Pd, since Pd in those samples has been preferentially lost. The positive and well-correlated relationship between Os and Ir in all samples, along with the correlation between Ir and Pd in samples with less than 4.5 wt% sulfur (Fig. 9), indicates that variability in the primary sulfide melt composition of the Huangshannan deposit is mainly controlled by R factor. Relatively low PGE tenors (10 ppb Os, 6 ppb Ir, 7 ppb Ru, 6 ppb Rh) and Ni tenor (~11 wt%) in olivine websterite with S content higher than 10 wt% indicate that these sulfides were segregated from relatively low R values (Fig. 7a). Modeling results of Ni tenors at variable R values (Fig. 12) indicate that these low PGE and Ni sulfides could be derived from R value at 600 if they were formed by sulfide-silicate melt equilibrium, or from R value at ~150 if they were formed by sulfide-silicate melt-olivine (20%) equilibrium. These R values and the PGE tenors are used to constrain the PGE concentrations in parental magma. In the first case that the sulfides were formed at R value of 600, the estimated Os, Ir, Ru, and Rh concentrations in the parental magma are 0.02 ppb, 0.012 ppb, 0.014 ppb, and 0.012 ppb respectively, representing the minimum PGE concentrations in parental magma. In the latter case, the calculated Os, Ir, Ru, and Rh concentrations are 0.07 ppb, 0.04 ppb, 0.05 ppb, 0.04 ppb respectively, representing the maximum PGE concentrations in the magma. In terms of the correlation between Ni and Os, Ir (Fig. 9) as well as correlations between PGE tenors (Fig. 7), 0.05 ppb Os, 0.023 ppb Ir, and 0.5 ppb Pd in the parental magma, coupled with R value varying from 200 to 3000, can explain the PGE tenors of the Huangshannan sulfides.

Magmas are most likely to form magmatic sulfide deposits of economic Ni-Cu-PGE grades if the sulfides are being physically entrained and transported in the form of sulfide liquid droplets prior to being mechanically deposited (Barnes et al., 2016). Applying the equation of Li and Ripley (2009), the calculated value of sulfur contents at sulfide saturation of the Huangshannan parental magma decreases from 1750 ppm to 1000 ppm after 20 wt% fractional crystallization of olivine and orthopyroxene (Mao et al., 2016), indicating the silicate-sulfide cotectic ratio is ~100 during olivine and orthopyroxene crystallization. This cotectic ratio corresponds to <0.7 wt% disseminated sulfide in lherzolite and olivine websterite, which is significantly lower than the sulfide proportion of the Huangshannan deposit (1 < S < 13 wt%). The supra-cotectic proportions of sulfide liquid to cumulus silicates in the Huangshannan ores, together with the relatively high R-values (150–3000, commonly > 600), implies mechanical transport and deposition of excess sulfide liquid in a

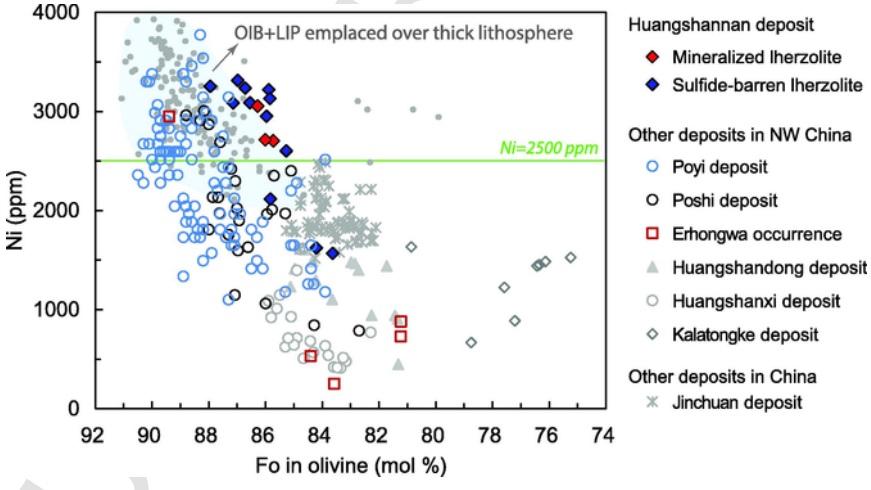

Fig. 13. The comparison between olivine composition of the Huangshannan deposit and those of other magmatic sulfide deposits regionally. Olivine composition from oceanic island basalt (OIB) and large igneous province (LIP) emplaced over thick lithosphere, which is believed to be related with Ni-rich magma (Sobolev et al., 2007) are also included for comparison. Data source is the same to these listed in Fig. 5 and A1. Microbeam XRF element distribution maps showing the proportions of the pentlandite, pyrrhotite, and chalcopyrite in the high Ni tenor sulfides hosted by olivine websterite. (a). Optical photomosaic of the cut surface; (b). Abundances are scaled to a maximum number of counts per element and shown as false-color three-channel RGB maps with Ni in the red channel, Cu in green, and S in blue. Olivine appears in dark gray and pyroxene appears in light gray and the separation of olivine and pyroxene is based on the abundances of Fe, Ca and Cr in the maps. (For interpretation of the references to colour in this figure legend, the reader is referred to the web version of this article.)

magma pathway or a conduit, in which sulfides would have interacted with large volumes of silicate magma, prior to being mechanically deposited in the cumulates.

6.4. A two stage contamination model indicated by decoupling of the Re-Os and S isotopes

Experimental work and many studies of giant magmatic ore deposits propose that sulfide liquid segregation was a consequence of assimilation of crust or crustal-derived sulfides into sulfide undersaturated magmas (Grinenko, 1985; Lambert et al., 2000; Mavrogenes and O'Neill, 1999). Crustal rocks tend to have distinctively high Re/Os ratios and very radiogenic Os isotopic compositions relative to mantle reservoirs (Lambert et al., 2000; Shirey and Walker, 1998). Thus, the Re-Os isotopic system is potentially a highly sensitive monitor of the extent of crustal involvement during ore genesis. Nevertheless, Os isotope anomalies become very rapidly diluted at high R factors, Os being a trace element in sulfide magma and an ultra-trace element in silicate magma (Lesher and Burnham, 2001). On the other hand, S isotopes provide a useful means of evaluating the source of sulfur in magmatic Ni-Cu deposits, owing to the relatively high concentrations of S in the sulfide magma compared to the silicate magma (Ripley and Li, 2003). Unusually, the sulfides from the Huangshannan deposit have elevated γOs values (at 278 Ma, 108–129) but mantle-like S isotope values (−0.4 to 0.8‰). Similarly, the majority of the Ni-Cu deposits in the Eastern Tianshan are characterized by high γOs values but restricted $\delta^{34}S$ values close to mantle values (Wang et al., 1987; Tang et al., 2012). This creates a problem for interpretation in terms of simple single stage contamination models: contamination-related Os isotopic anomalies should become diluted at lower R factors than S isotope signals, owing to the much higher ratio of Os in the magma to Os in the contaminant relative to the equivalent ratio for S (Lesher and Burnham, 2001; Ripley and Li, 2003).

Yang et al. (2013b) proposed that sulfide saturation of the Poyi and Poshi deposits in the Beishan Terrane was triggered by the assimilation of crustal sulfides with both high γOs and Re/Os ratios, on the grounds that sulfides in these deposits have high γOs (at 280 Ma) values (+30 to +292) that are negatively correlated with the abundance of Os in 100% sulfides and positively correlated with Re/Os ratios. In the case of the Eastern Tianshan, sulfides of the wall rock of these Ni-Cu deposits have $\delta^{34}S$ values ranging from 1.9 to 7.2‰ (Tang et al., 2012). We apply the equation 8 of Lesher and Burnham (2001) to estimate the effect of such wall rock sulfide addition, assuming mantle-derived melt has 0.1 ppb Os, $^{187}Os/^{188}Os_i$ of 0.14 (Shirey and Walker, 1998) and that wall rock sulfides contain 50 ppb Re, 1.2 ppb Os, and $^{187}Os/^{188}Os_i$ of 1.93 at 278 Ma (Yang et al., 2013b). Modeling results indicate that sulfide contamination from wall rocks not only increases the γOs values but also increases the $\delta^{34}S$ values from 0‰ to 1.3–5‰, which are higher than these of the Huangshannan deposit (-0.4 to 0.8‰, Fig. 11b).

A possible solution to this problem is that the Os isotopic signature of the magma was modified by an earlier stage of crustal contamination, prior to the assimilation event that induced sulfide saturation. Assuming that the lower crust of the Eastern Tianshan has similar composition to the average lower crust composition which containing 0.1 ppb Os, has $^{187}Os/^{188}Os_i$ of 0.8 (Saal et al., 1998), and a $\delta^{34}S$ value of 0‰, and that sulfides in wall rocks contain 1.2 ppb Os, have $^{187}Os/^{188}Os_i$ of 1.93 (Yang et al., 2013b), and $\delta^{34}S$ values of 1.9–7.2‰ (Tang et al., 2012) at the age of 278 Ma (Mao et al., 2016), mixing modeling indicates that addition of ∼20% lower crustal components plus a lower proportion of upper crustal sulfide (high R value circumstance) to the parental magma can result in the observed Os-S isotopic composition (Fig. 11). The assimilation event at high R factor generates a sulfide melt with high Ni tenor and radiogenic Os signal, inherited from the pre-contaminated silicate magma. This two stage contamination model is consistent with the previous study on Sr-Nd-Hf-O isotopes (Mao et al., 2016).

6.5. Implications for high Ni tenor magmatic sulfide deposit exploration in NW China

Sulfide fractionation during intercumulus percolation is indicted by the relative Pt and Pd depletion in the more sulfide-rich ores. This implies that Pt (Pd)-Cu enriched segregated sulfide ores might occur in the certain part of the intrusion.

Besides the Huangshannan intrusion, the Poyi, Poshi and other intrusions in Beishan are characterized by large volumes of olivine, which are relatively enriched in Ni (Su et al., 2011b; Xue et al., 2016). The Erhongwa intrusion also has large proportion of Ni-rich olivine in sulfide-poor rocks (Fig. 13) (Sun et al., 2013a). However, no high Ni tenor sulfides have been reported to date. The presence of Ni-rich olivine indicates that the Poyi and Poshi deposits cannot be explained by deposition of sulfides after extensive olivine crystallization. Indeed, sulfides in these intrusions were formed at high R-values and sulfide segregation took place at the beginning of olivine fractionation (Xue et al., 2016; Yang et al., 2013b). Thus, it appears some Ni-rich sulfides may remain hidden in unexposed portions of both the Poyi and the Poshi intrusions.

7. Conclusions

Based on the data presented here, and on a comparison between the Huangshannan deposit and other deposits in the region, new findings and interpretations are summarized as follows:

1. The sulfides of the ultramafic rocks from the Huangshannan deposit are characterized by high Ni tenor, the highest known in the Central Asian Orogenic Belt.
2. Mechanical transport and deposition of excess sulfide liquid in a magma pathway or a conduit played an important role in forming the deposit.
3. High Ni tenor is the result of olivine-sulfide-silicate liquid equilibrium at high R values from a relatively Ni-rich parental magma.
4. Pt and Pd depletion are attributed to sulfide liquid fractionation coupled with Cu-rich sulfide liquid percolation.
5. Contamination by lower crustal material at depth, without the generation of large proportions of sulfide liquid, and subsequent addition of sulfides from the immediate wall rocks to the intrusion account for decoupling of Os and S isotopic signals in the opposite sense from that expected by a single stage sulfide-generating contamination event.
6. Regionally, mafic-ultramafic intrusions with Ni-rich olivines, such as the Poyi and Poshi bodies, have exploration potential for high Ni tenor ores.

8. Uncited references

Barnes et al. (2015), Gao and Zhou (2013), Lambert et al. (1999), Tang et al. (2014).

Acknowledgements

This study has been financially supported by grants from Nature Science Foundation of China (grant 41502095, 41030424 and

41472075), China Postdoctoral Science Foundation (2015M570146 Ya–Jing Mao) and the Xinjiang Nonferrous Metal Industry Group Ltd. It was supported by resources provided by the Pawsey Supercomputing Centre with funding from the Australian Government and the Government of Western Australia. We thank Guan–Liang Ren, Xiao–Dong Zhang, Jun–Hui Xie, Ding–Min Guo for their assistance in field work, and Chusi Li, Edward M. Ripley and Liang Qi for their assistance in laboratory work. This manuscript is completed during the visit of Ya–Jing Mao to CSIRO as a post–doctoral fellow, funded by the China Scholarship Council. SJB and MLV acknowledge support from the CSIRO Science Plus Science Leader program. The clarity of the manuscript was significantly improved by comments from James Scoates, Zhuangzhi Qian and anonymous reviewers. Editors of the special issue, Marco Fiorentini and David R. Mole, are thanked for editorial handling.

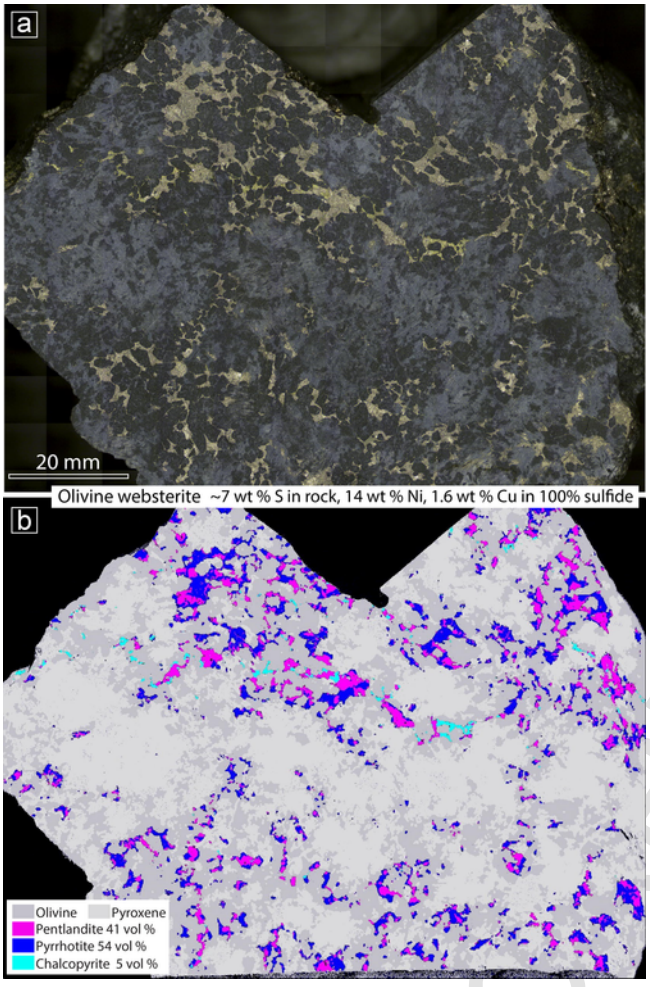

Fig. A1. Microbeam XRF element distribution maps showing the proportions of the pentlandite, pyrrhotite, and chalcopyrite in the high Ni tenor sulfides hosted by olivine websterite. (a). Optical photomosaic of the cut surface; (b). Abundances are scaled to a maximum number of counts per element and shown as false-color three-channel RGB maps with Ni in the red channel, Cu in green, and S in blue. Olivine appears in dark gray and pyroxene appears in light gray and the separation of olivine and pyroxene is based on the abundances of Fe, Ca and Cr in the maps. (For interpretation of the references to colour in this figure legend, the reader is referred to the web version of this article.)

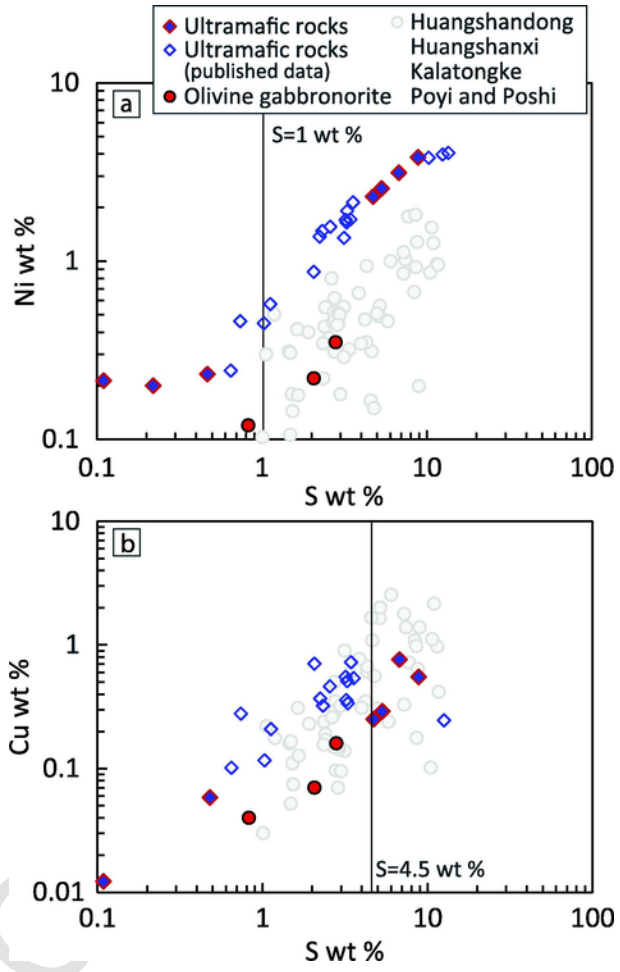

Fig. A2. Plot of Ni (a) and Cu (b) versus S contents in whole rock samples from the Huangshannan deposit as well as other deposits regionally. Data source: Huangshannan deposit (this study, Zhao et al., 2015), Other deposits: Huangshandong (Gao et al., 2013; Mao et al., 2015), Huangshanxi (Mao et al., 2014a; Zhang et al., 2011), Kalatongke (Song and Li, 2009), Poyi and Poshi deposits (Yang et al., 2013b).Fig. A3. Plot of PGE versus S contents in whole rock samples from the Huangshannan deposit. Positive correlations between Os, Ir, Rh, Rh and S (a–d) are shown for ultramafic samples with less than 10 wt% sulfur, whereas positive correlations between Pt, Pd and S are merely shown for samples with <4.5 wt% sulfur. Data source is the same to these listed in Fig. A2.

Appendix A.

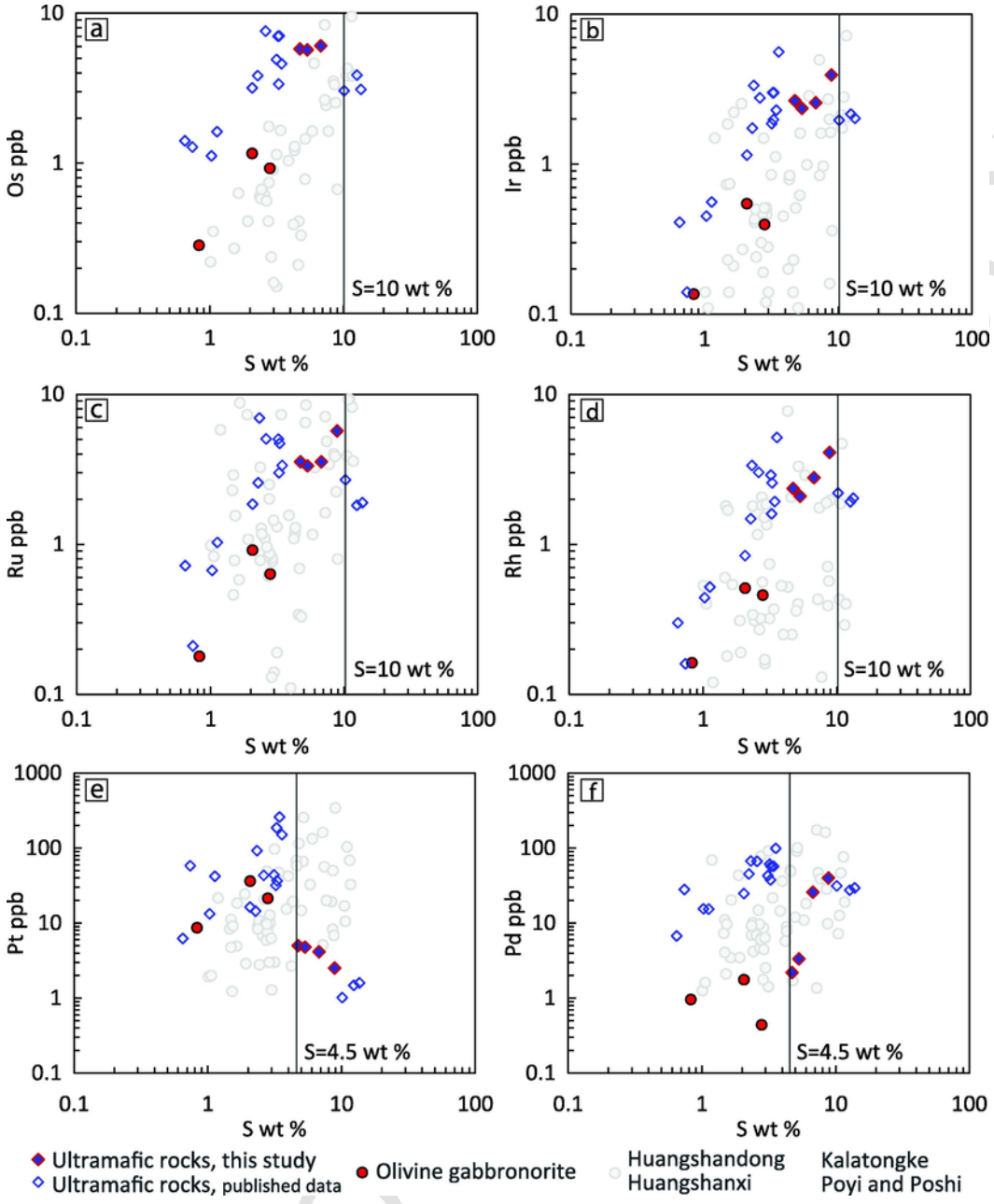

Fig. A3. Plot of PGE versus S contents in whole rock samples from the Huangshannan deposit. Positive correlations between Os, Ir, Rh, Rh and S (a–d) are shown for ultramafic samples with less than 10 wt% sulfur, whereas positive correlations between Pt, Pd and S are merely shown for samples with <4.5 wt% sulfur. Data source is the same to these listed in Fig. A2.

References

Ao, S.J., Xiao, W.J., Han, C.M., Mao, Q.G., Zhang, J.E., 2010. Geochronology and geochemistry of Early Permian mafic–ultramafic complexes in the Beishan area, Xinjiang, NW China: implications for late Paleozoic tectonic evolution of the southern Altaids. Gondwana Res. 18, 466–478.

Barnes, S. J., 2006, Komatiite-hosted nickel sulfide deposits: geology, geochemistry, and genesis. In Barnes, S.J., (Ed.), Nickel Deposits of the Yilgarn Craton: Geology, Geochemistry, and Geophysics Applied to Exploration: Colorado, Special Publication-Society of Economic Geologist, 13, p. 51–118.

Barnes, S.J., Liu, W., 2012. Pt and Pd mobility in hydrothermal fluids: evidence from komatiites and from thermodynamic modelling. Ore Geol. Rev. 44, 49–58.

Barnes, S.-J., Maier, W., 1999. The fractionation of Ni, Cu and the noble metals in silicate and sulphide liquids. Geol. Assoc. Can. Short Course Notes 13, 69–106.

Barnes, S.J., Gole, M.J., Hill, R.E.T., 1988. The Agnew Nickel Deposit, Western Australia: part II. Sulfide geochemistry, with emphasis on the platinum-group elements. Econ. Geol. 83, 537–550.

Barnes, S.-J., Lightfoot, P., 2005, Formation of magmatic nickel-sulfide ore deposits and processes affecting their copper and platinum-group element contents. In: Thompson, J.F.H., Goldfarb, R.J., Richards, J.P., (Eds.), Economic Geology 100th Anniversary Volume, Society of Economic Geologists, pp. 179–213.

Barnes, S.J., Osborne, G.A., Cook, D., Barnes, L., Maier, W.D., Godel, B., 2011. The Santa Rita nickel sulfide deposit in the Fazenda Mirabela intrusion, Bahia, Brazil: Geology, sulfide geochemistry, and genesis. Econ. Geol. 106, 1083–1110.

Barnes, S.J., Godel, B.M., Locmelis, M., Fiorentini, M.L., Ryan, C.G., 2011. Extremely Ni-rich Fe-Ni sulfide assemblages in komatiitic dunite at Betheno, Western Australia: results from synchrotron X-ray fluorescence mapping. Aust. J. Earth Sci. 58, 691–709.

Barnes, S.J., Godel, B., Gürer, D., Brenan, J.M., Robertson, J., Paterson, D., 2013. Sulfide-olivine Fe-Ni exchange and the origin of anomalously Ni rich magmatic sulfides. Econ. Geol. 108, 1971–1982.

Barnes, S.J., Cruden, A.R., Arndt, N., Saumur, B.M., 2016. The mineral system approach applied to magmatic Ni–Cu–PGE sulphide deposits. Ore Geol. Rev. 76, 296–316.

Barnes, S. J., Mungall, J. E., Le Vaillant, M., Godel, B., Lesher, C. M., Holwell, D., Lightfoot, P. C., Krivolutskaya, N. and Wei, B. Sulfide-silicate textures in magmatic Ni-Cu-PGE sulfide ore deposits: Disseminated and net-textured ores. Am Mineral. **102**, 2017, 473-506.

BGMRXUAR (Bureau of Geology and Mineral Resources of Xinjiang Uygur Autonomous Region), 1993. Regional Geology of Xinjiang Uygur Autonomous Region. Geological Publishing House, Beijing. 1-841p.

Brenan, J.M., Caciagli, N.C., 2000. Fe–Ni exchange between olivine and sulphide liquid: implications for oxygen barometry in sulphide-saturated magmas. Geochim. Cosmochim. Acta 64, 307–320.

Campbell, I.H., Naldrett, A.J., 1979. The influence of silicate:sulfide ratios on the geochemistry of magmatic sulfides. Econ. Geol. 74, 1503–1506.

Chai, G., Naldrett, A., 1992. The Jinchuan Ultramafic Intrusion: Cumulate of a High-Mg Basaltic Magma. J. Petrol. 33, 277–303.

Chai, F., Zhang, Z., Mao, J., Dong, L., Zhang, Z., Wu, H., 2008. Geology, petrology and geochemistry of the Baishiquan Ni–Cu-bearing mafic–ultramafic intrusions in Xinjiang, NW China: Implications for tectonics and genesis of ores. J. Asian Earth Sci. 32, 218–235.

Chung, H.-Y., Mungall, J.E., 2009. Physical constraints on the migration of immiscible fluids through partially molten silicates, with special reference to magmatic sulfide ores. Earth Planet. Sci. Lett. 286, 14–22.

Deng, Y.-F., Song, X.-Y., Chen, L.-M., Zhou, T., Pirajno, F., Yuan, F., Xie, W., Zhang, D., 2014. Geochemistry of the Huangshandong Ni–Cu deposit in northwestern China: Implications for the formation of magmatic sulfide mineralization in orogenic belts. Ore Geol. Rev. 56, 181–198.

Donaldson, M.J., 1981. Redistribution of ore elements during serpentinization and talc-carbonate alteration of some Archean dunites, Western Australia. Econ. Geol. 76, 1698–1713.

Du, A., Wu, S., Sun, D., Wang, S., Qu, W., Markey, R., Stain, H., Morgan, J., Malinovskiy, D., 2004. Preparation and Certification of Re-Os Dating Reference Materials: Molybdenites HLP and JDC. Geostand. Geoanal. Res. 28, 41–52.

Gao, J.-F., Zhou, M.-F., Lightfoot, P.C., Wang, C.Y., Qi, L., Sun, M., 2013. Sulfide Saturation and Magma Emplacement in the Formation of the Permian Huangshandong Ni-Cu Sulfide Deposit, Xinjiang, Northwestern China. Econ. Geol. 108, 1833–1848.

Godel, B., Barnes, S.-J., Maier, W.D., 2007. Platinum-Group Elements in Sulphide Minerals, Platinum-Group Minerals, and Whole-Rocks of the Merensky Reef (Bushveld Complex, South Africa): Implications for the Formation of the Reef. J. Petrol. 48, 1569–1604.

Godel, B., Barnes, S.J., Barnes, S.-J., Maier, W.D., 2010. Platinum ore in three dimensions: Insights from high-resolution X-ray computed tomography. Geology 38, 1127–1130.

Grinenko, L., 1985. Sources of sulfur of the nickeliferous and barren gabbro-dolerite intrusions of the northwest Siberian platform. Int. Geol. Rev. 27, 695–708.

Han, B.F., Ji, J.Q., Song, B., Chen, L.H., Li, Z., 2004. SHRIMP zircon U-Pb ages of kalatongke No. 1 and Huangshandong Cu-Ni-bearing mafic-ultramafic complexes, North Xinjiang, and geological implications. Chin. Sci. Bull. 49, 2424–2429.

Han, C.M., Xiao, W.J., Zhao, G.C., Ao, S.J., Zhang, J.E., Qu, W.J., Du, A.D., 2010. In-situ U-Pb, Hf and Re-Os isotopic analyses of the Xiangshan Ni-Cu-Co deposit in Eastern Tianshan (Xinjiang), Central Asia Orogenic Belt Constraints on the timing and genesis of the mineralization. Lithos 120, 547–562.

Han, C.M., Xiao, W.J., Zhao, G.C., Su, B.X., Sakyi, P.A., Ao, S.J., Wan, B., Zhang, J.E., Zhang, Z.Y., 2013. SIMS U-Pb zircon dating and Re-Os isotopic analysis of the Hulu Cu-Ni deposit, eastern Tianshan, Central Asian Orogenic Belt, and its geological significance. J. Geosci. 58, 251–270.

Hanski, E.J., Luo, Z., Oduro, H., Walker, R.J., 2011. The Pechenga Ni-Cu sulfide deposits, northwestern Russia: A review with new constraints from the feeder dikes. Econ. Geol. 17, 145–162.

Jahn, B.M., 2004. The central Asian orogenic belt and growth of the continental crust in the phanerozoic: Aspects of the Tectonic Evolution of China, vol. 226, pp. 73–100.

Keays, R.R., 1995. The role of komatiitic and picritic magmatism and S-saturation in the formation of ore deposits. Lithos 34, 1–18.

Konnunaho, J.P., Hanski, E.J., Bekker, A., Halkoaho, T.A.A., Hiebert, R.S., Wing, B.A., 2013. The Archean komatiite-hosted, PGE-bearing Ni-Cu sulfide deposit at Vaara, eastern Finland: evidence for assimilation of external sulfur and post-depositional desulfurization. Miner. Deposita 48, 967–989.

Lambert, D.D., Frick, L.R., Foster, J.G., Li, C., Naldrett, A.J., 2000. Re-Os Isotope Systematics of the Voisey's Bay Ni-Cu-Co Magmatic Sulfide System, Labrador, Canada: II. Implications for Parental Magma Chemistry, Ore Genesis, and Metal Redistribution. Econ. Geol. 95, 867–888.

Le Vaillant, M., Barnes, S.J., Fiorentini, M.L., Santaguida, F., Törmänen, T., 2016. Effects of hydrous alteration on the distribution of base metals and platinum group elements within the Kevitsa magmatic nickel sulphide deposit. Ore Geol. Rev. 72 Part 1, 128–148.

Lesher, C.M., Burnham, O.M., 2001. Multicomponent elemental and isotopic mixing in Ni–Cu–(PGE) ores at Kambalda, Western Australia. Can. Mineral. 39, 421–446.

Lesher, C., and Keays, R., 2002, Komatiite-associated Ni-Cu-PGE deposits: Geology, mineralogy, geochemistry and genesis, Canadian Institute Mineral Metallurgy Petroleum.

Li, C., Ripley, E.M., 2009. Sulfur contents at sulfide-liquid or anhydrite saturation in silicate melts: empirical equations and example applications. Econ. Geol. 104, 405–412.

Li, C., Zhang, M.J., Fu, P., Qian, Z.Z., Hu, P.Q., Ripley, E.M., 2012. The Kalatongke magmatic Ni-Cu deposits in the Central Asian Orogenic Belt, NW China: product of slab window magmatism?. Miner. Deposita 47, 51–67.

Li, C., Zhang, Z., Li, W., Wang, Y., Sun, T., Ripley, E.M., 2015. Geochronology, petrology and Hf–S isotope geochemistry of the newly-discovered Xiarihamu magmatic Ni–Cu sulfide deposit in the Qinghai-Tibet plateau, western China. Lithos 216–217, 224–240.

Lightfoot, P.C., Evans-Lamswood, D., 2015. Structural controls on the primary distribution of mafic–ultramafic intrusions containing Ni–Cu–Co–(PGE) sulfide mineralization in the roots of large igneous provinces. Ore Geol. Rev. 64, 354–386.

Mao, J.W., Pirajno, F., Zhang, Z.H., Chai, F.M., Wu, H., Chen, S.P., Cheng, L.S., Yang, J.M., Zhang, C.Q., 2008. A review of the Cu-Ni sulphide deposits in the Chinese Tianshan and Altay orogens (Xinjiang Autonomous Region, NW China): Principal characteristics and ore-forming processes. J. Asian Earth Sci. 32, 184–203.

Mao, Y.-J., Qin, K.-Z., Li, C., Xue, S.C., Ripley, E.M., 2014. Petrogenesis and ore genesis of the Permian Huangshanxi sulfide ore-bearing mafic-ultramafic intrusion in the Central Asian Orogenic Belt, western China. Lithos 200, 111–125.

Mao, Y.-J., Qin, K.-Z., Tang, D.M., Xue, S.C., Feng, H.Y., Tian, Y., 2014. Multiple stages of magma emplacement and mineralization of eastern Tianshan, Xinjiang: exemplified by the Huangshan Ni-Cu deposit. Acta Petrol. Sin. 30, 1575–1594.

Mao, Y.-J., Qin, K.-Z., Li, C., Tang, D.-M., 2015. A modified genetic model for the Huangshandong magmatic sulfide deposit in the Central Asian Orogenic Belt, Xinjiang, western China. Mineral. Deposita 50, 65–82.

Mao, Y.-J., Qin, K.-Z., Tang, D.-M., Feng, H.-Y., Xue, S.-C., 2016. Crustal contamination and sulfide immiscibility history of the Permian Huangshannan magmatic Ni-Cu sulfide deposit, East Tianshan, NW China. J. Asian Earth Sci.

Mavrogenes, J.A., O'Neill, H.S.C., 1999. The relative effects of pressure, temperature and oxygen fugacity on the solubility of sulfide in mafic magmas. Geochim. Cosmochim. Acta 63, 1173–1180.

Mungall, J.E., 2002. Late-Stage Sulfide Liquid Mobility in the Main Mass of the Sudbury Igneous Complex: Examples from the Victor Deep, McCreedy East, and Trillabelle Deposits. Econ. Geol. 97, 1563–1576.

Mungall, J.E., Brenan, J.M., 2014. Partitioning of platinum-group elements and Au between sulfide liquid and basalt and the origins of mantle-crust fractionation of the chalcophile elements. Geochim. Cosmochim. Acta 125, 265–289.

Naldrett, A.J., Innes, D.G., Sowa, J., Gorton, M.P., 1982. Compositional Variations within and between five Sudbury Ore-Deposits. Econ. Geol. 77, 1519–1534.

Naldrett, A.J., Ebel, D.S., Asif, M., Morrison, G., Moore, C.M., 1997. Fractional crystallisation of sulfide melts as illustrated at Noril'sk and Sudbury. Eur. J. Mineral. 9, 365–377.

Qi, L., Zhou, M.-F., Wang, C.Y., Sun, M., 2007. Evaluation of a technique for determining Re and PGEs in geological samples by ICP-MS coupled with a modified Carius tube digestion. Geochem. J. 41, 407–414.

Qian, Z.Z., Wang, J.Z., Jiang, C.Y., Jiao, J.G., Yan, H.Q., He, K., Sun, T., 2009. Geochemistry characters of platinum-group elements and its significances on the process of mineralization in the Kalatongke Cu-Ni sulfide deposit, Xinjiang, China. Acta Petrol. Sin. 25, 832–844.

Qin, K.-Z., Su, B.-X., Sakyi, P.A., Tang, D.M., Li, X.H., Sun, H., Xiao, Q.H., Liu, P.P., 2011. Sims zircon U-Pb geochronology and Sr-Nd isotopes of Ni-Cu-bearing mafic-ultramafic intrusions in Eastern tianshan and Beishan in correlation with flood basalts in Tarim basin (NW China): Constraints on a Ca. 280 Ma mantle plume. Am. J. Sci. 311, 237–260.

Ripley, E.M., Li, C., 2003. Sulfur isotope exchange and metal enrichment in the formation of magmatic Cu-Ni-(PGE) deposits. Econ. Geol. 98, 635–641.

Saal, A.E., Rudnick, R.L., Ravizza, G.E., Hart, S.R., 1998. Re-Os isotope evidence for the composition, formation and age of the lower continental crust. Nature 393, 58–61.

Sciortino, M., Mungall, J.E., Muinonen, J., 2015. Generation of High-Ni Sulfide and Alloy Phases During Serpentinization of Dunite in the Dumont Sill, Quebec. Econ. Geol. 110, 733–761.

Shirey, S.B., Walker, R.J., 1998. The Re-Os isotope system in cosmochemistry and high-temperature geochemistry. Annu. Rev. Earth Planet. Sci. 26, 423–500.

Sobolev, A.V., Hofmann, A.W., Kuzmin, D.V., Yaxley, G.M., Arndt, N.T., Chung, S.L., Danyushevsky, L.V., Elliott, T., Frey, F.A., Garcia, M.O., Gurenko, A.A.,

Kamenetsky, V.S., Kerr, A.C., Krivolutskaya, N.A., Matvienkov, V.V., Nikogosian, I.K., Rocholl, A., Sigurdsson, I.A., Sushchevskaya, N.M., Teklay, M., 2007. The amount of recycled crust in sources of mantle-derived melts. Science 316, 412–417.

Song, X.-Y., Li, X.R., 2009. Geochemistry of the Kalatongke Ni-Cu-(PGE) sulfide deposit, NW China: implications for the formation of magmatic sulfide mineralization in a postcollisional environment. Mineral. Deposita 44, 303–327.

Song, X.-Y., Zhou, M.-F., Cao, Z.-M., Sun, M., Wang, Y.-L., 2003. Ni–Cu–(PGE) magmatic sulfide deposits in the Yangliuping area, Permian Emeishan igneous province, SW China. Miner. Deposita 38, 831–843.

Song, X.-Y., Keays, R.R., Zhou, M.-F., Qi, L., Ihlenfeld, C., Xiao, J.-F., 2009. Siderophile and chalcophile elemental constraints on the origin of the Jinchuan Ni-Cu-(PGE) sulfide deposit, NW China. Geochim. Cosmochim. Acta 73, 404–424.

Song, X.-Y., Chen, L.-M., Deng, Y.-F., Xie, W., 2013. Syncollisional tholeiitic magmatism induced by asthenosphere upwelling owing to slab detachment at the southern margin of the Central Asian Orogenic Belt. J. Geol. Soc. 170, 941–950.

Song, X.-Y., Chen, L.M., Deng, Y.F., Xie, W., 2013. Syncollisional tholeiitic magmatism induced by asthenosphere upwelling owing to slab detachment at the southern margin of the Central Asian Orogenic Belt. J. Geol. Soc. 170, 941–950.

Song, X.-Y., Yi, J.-N., Chen, L.-M., She, Y.-W., Liu, C.-Z., Dang, X.-Y., Yang, Q.-A., Wu, S.-K., 2016. The Giant Xiarihamu Ni-Co Sulfide Deposit in the East Kunlun Orogenic Belt, Northern Tibet Plateau, China. Econ. Geol. 111, 29–55.

Studley, S.A., Ripley, E.M., Elswick, E.R., Dorais, M.J., Fong, J., Finkelstein, D., Pratt, L.M., 2002. Analysis of sulfides in whole rock matrices by elemental analyzer–continuous flow isotope ratio mass spectrometry. Chem. Geol. 192, 141–148.

Su, B.-X., Qin, K.-Z., Sakyi, P.A., Li, X.-H., Yang, Y.-H., Sun, H., Tang, D.-M., Liu, P.-P., Xiao, Q.-H., Malaviarachchi, S.P.K., 2011. U-Pb ages and Hf–O isotopes of zircons from Late Paleozoic mafic–ultramafic units in the southern Central Asian Orogenic Belt: Tectonic implications and evidence for an Early-Permian mantle plume. Gondwana Res. 20, 516–531.

Su, B.-X., Qin, K.-Z., Tang, D.-M., Deng, G., Xiao, Q.-H., Sun, H., Lu, H.-F., Dai, Y.-C., 2011. Petrological features and implications for mineralization of the Poshi mafic-ultramafic intrusion in Beishan area, Xinjiang. Acta Petrol. Sin. 27, 3627–3639.

Sun, T., Qian, Z.-Z., Li, C., Xia, M.-Z., Yang, S.-H., 2013. Petrogenesis and economic potential of the Erhongwa mafic–ultramafic intrusion in the Central Asian Orogenic Belt, NW China: Constraints from olivine chemistry, U-Pb age and Hf isotopes of zircons, and whole-rock Sr–Nd–Pb isotopes. Lithos 182–183, 185–199.

Sun, T., Qian, Z.Z., Deng, Y.F., Li, C.S., Song, X.Y., Tang, Q.Y., 2013. PGE and Isotope (Hf-Sr-Nd-Pb) Constraints on the Origin of the Huangshandong Magmatic Ni-Cu Sulfide Deposit in the Central Asian Orogenic Belt, Northwestern China. Econ. Geol. 108, 1849–1864.

Tang, D., Qin, K., Li, C., Qi, L., Su, B., Qu, W., 2011. Zircon dating, Hf–Sr–Nd–Os isotopes and PGE geochemistry of the Tianyu sulfide-bearing mafic–ultramafic intrusion in the Central Asian Orogenic Belt, NW China. Lithos 126, 84–98.

Tang, D.M., Qin, K.Z., Sun, H., Su, B.X., Xiao, Q.H., 2012. The role of crustal contamination in the formation of Ni-Cu sulfide deposits in Eastern Tianshan, Xinjiang, Northwest China: Evidence from trace element geochemistry, Re-Os, Sr-Nd, zircon Hf-O, and sulfur isotopes. J. Asian Earth Sci. 49, 145–160.

Tao, Y., Li, C., Song, X.-Y., Ripley, E., 2008. Mineralogical, petrological, and geochemical studies of the Limahe mafic–ultramatic intrusion and associated Ni–Cu sulfide ores, SW China. Mineral. Deposita 43, 849–872.

Wang, R., Zhao, C., 1991. Intrusion 1 of the Kalatongke Magmatic Ni-Cu Deposit. Geological Publication, Xinjiang, Beijing.

Wang, R.M., Liu, D.Q., Yin, D.T., 1987. The conditions of controlling metallogny of Cu-Ni sulfide ore deposits and the orientation of finding ore Hami, Xinjiang, China. J. Mineral. Petrol. 7, 1–152.

Wang, C.Y., Zhou, M.F., Keays, R.R., 2006. Geochemical constraints on the origin of the Permian Baimazhai mafic-ultramafic intrusion, SW China. Contrib. Miner. Petrol. 152, 309–321.

Wu, F.-Y., Wilde, S.A., Zhang, G.-L., Sun, D.-Y., 2004. Geochronology and petrogenesis of the post-orogenic Cu–Ni sulfide-bearing mafic–ultramafic complexes in Jilin Province, NE China. J. Asian Earth Sci. 23, 781–797.

Xiao, W.J., Windley, B.F., Huang, B.C., Han, C.M., Yuan, C., Chen, H.L., Sun, M., Sun, S., Li, J.L., 2009. End-Permian to mid-Triassic termination of the accretionary processes of the southern Altaids: implications for the geodynamic evolution, Phanerozoic continental growth, and metallogeny of Central Asia. Int. J. Earth Sci. 98, 1189–1217.

Xue, S., Qin, K., Li, C., Tang, D., Mao, Y., Qi, L., Ripley, E.M., 2016. Geochronological, Petrological and Geochemical Constraints on Ni-Cu Sulfide Mineralization in the Poyi Ultramafic-troctolitic Intrusion in the NE Rim of Tarim Craton, Western China. Econ. Geol.

Yang, S.-H., Zhou, M.-F., 2009. Geochemistry of the ~430-Ma Jingbulake mafic–ultramafic intrusion in Western Xinjiang, NW China: Implications for subduction related magmatism in the South Tianshan orogenic belt. Lithos 113, 259–273.

Yang, S.-H., Maier, W., Hanski, E., Lappalainen, M., Santaguida, F., Määttä, S., 2013. Origin of ultra-nickeliferous olivine in the Kevitsa Ni–Cu–PGE-mineralized intrusion, northern Finland. Contrib. Miner. Petrol. 166, 81–95.

Yang, S.-H., Zhou, M.-F., Lightfoot, P.C., Xu, J.-F., Wang, C.Y., Jiang, C.-Y., Qu, W.-J., 2013. Re–Os isotope and platinum-group element geochemistry of the Pobei Ni–Cu sulfide-bearing mafic–ultramafic complex in the northeastern part of the Tarim Craton. Miner. Deposita 49, 381–397.

Zhang, Z.C., Mao, J.W., Chai, F.M., Yan, S.H., Chen, B.L., Pirajno, F., 2009. Geochemistry of the Permian Kalatongke Mafic Intrusions, Northern Xinjiang, Northwest China: Implications for the Genesis of Magmatic Ni-Cu Sulfide Deposits. Econ. Geol. 104, 185–203.

Zhang, M., Li, C., Fu, P., Hu, P., Ripley, E., 2011. The Permian Huangshanxi Cu–Ni deposit in western China: intrusive–extrusive association, ore genesis, and exploration implications. Miner. Deposita 46, 153–170.

Zhao, Y., Xue, C., Zhao, X., Yang, Y., Ke, J., 2015. Magmatic Cu–Ni sulfide mineralization of the Huangshannan mafic–untramafic intrusion, Eastern Tianshan, China. J. Asian Earth Sci. 105, 155–172.

Zhou, M.F., Lesher, C.M., Yang, Z.X., Li, J.W., Sun, M., 2004. Geochemistry and petrogenesis of 270 Ma Ni-Cu-(PGE) sulfide-bearing mafic intrusions in the Huangshan district, Eastern Xinjiang, Northwest China: implications for the tectonic evolution of the Central Asian orogenic belt. Chem. Geol. 209, 233–257.